

Supporting Information

The Stereochemistry of the Reactions between Palladacycle Complexes and Primary Alkyl Iodides

Xinyu Xu and Lei Jiao*

Center of Basic Molecular Science (CBMS), Department of Chemistry,

Tsinghua University, Beijing, 100084 (China)

**E-mail: Leijiao@mail.tsinghua.edu.cn.*

Contents

1. General Information.	S2
2. Stereochemical Probe Synthesis.	S3
2.1 <i>t</i> -Bu Substituted Stereochemical Probe 1	S3
2.2 TBS Protected Stereochemical Probe 2	S4
2.3 Epimerization of Stereochemical Probes.	S7
3. Undeuterated Alkylation Product Synthesis.	S9
4. Stereochemical Investigations.	S12
4.1 Norbornene Derived Palladacycle Complex 3	S12
4.2 Alkene-ligand derived Palladacycle Complex 4	S12
4.3 Pyridine Coordinated Palladacycle Complex 5	S17
4.4 8-aminoquinoline Coordinated Palladacycle Complex 6	S18
5. DFT Calculations.	S20
5.1 Computational Methods.	S20
5.2 Geometry Structures of Alkylation Transition States.	S21
5.3 Orbital Energy Level Calculations.	S25
5.4 Natural Population Analysis and Charge Decomposition Analysis.	S26
5.5 Ligand Substitution Equilibrium of Complex 5	S28
6. NMR Spectra.	S30
References.	S40

1. General Information

Experimental. Air- and moisture-sensitive reactions were carried out under the protection of argon atmosphere. Reactions were stirred using Teflon-coated magnetic stir bars. Elevated temperatures were maintained using Thermostat-controlled metal or silicone oil baths. Organic solutions were concentrated using a rotary evaporator with a diaphragm vacuum pump. Analytical TLC was performed on silica gel GF₂₅₄ plates. The TLC plates were visualized by either ultraviolet light ($\lambda = 254$ nm) or a KMnO₄ stain. Purification of products was accomplished by flash column chromatography on silica gel (Innochem SilicaFlashP60, 230-400 mesh).

Chemicals. Pd(OAc)₂ was purchased from Energy Chemical, Pd(MeCN)₂Cl₂ was purchased from Innochem, Pd(PPh₃)₄ was purchased from Bidepharm. Reagent-grade tetrahydrofuran (THF), acetonitrile (MeCN), dichloromethane (DCM), toluene and diethyl ether (Et₂O) were purified by MBRAUN SPS 800 solvent purification system prior to use. Other solvents were purchased from J&K Scientific or Innochem as anhydrous solvent and were used as received. Other chemicals were purchased from various commercial sources and were used as received. Known compounds such as **1**¹, **3**², **5**³, **6**⁴, **7**⁵, **S1**⁶, **S2**⁶, **S6**⁷, Cp₂Zr(H)Cl⁸ and Cp₂Zr(D)Cl⁸ were synthesized according to literature methods and spectroscopic data matched those reported. The identity of deuterated alkylation products were confirmed by comparing the ¹H NMR spectra with their undeuterated derivatives.

Analytical. NMR spectra were recorded on a Bruker AVANCE III HD 400 (¹H at 400 MHz, ¹³C at 100 MHz) nuclear magnetic resonance spectrometer. The ¹H NMR spectra were calibrated against the peak of tetramethylsilane (TMS, 0 ppm), the ¹³C NMR spectra were calibrated against the peak of CDCl₃ (77.0 ppm). Diastereomeric ratio of stereochemical probes and alkylation products were determined by simulating their ¹H{²H} (with inverse gated 2H decoupling) NMR spectra. Infrared (IR) spectra were recorded on a Bruker FT-IR alpha (ATR mode) spectrophotometer.

2. Stereochemical Probe Synthesis

2.1 *t*-Bu Substituted Stereochemical Probe 1

t-Bu substituted stereochemical probe **1** was synthesized according to the literature method that reported by Gladysz group (Figure S1a).¹ A ca. 5 : 1 diastereomeric ratio was determined for our synthesized sample by simulation the corresponding $^1\text{H}\{^2\text{H}\}$ NMR spectra at the region of 3.11-3.19 ppm (H_1 of compound **1**; Figure S1b).

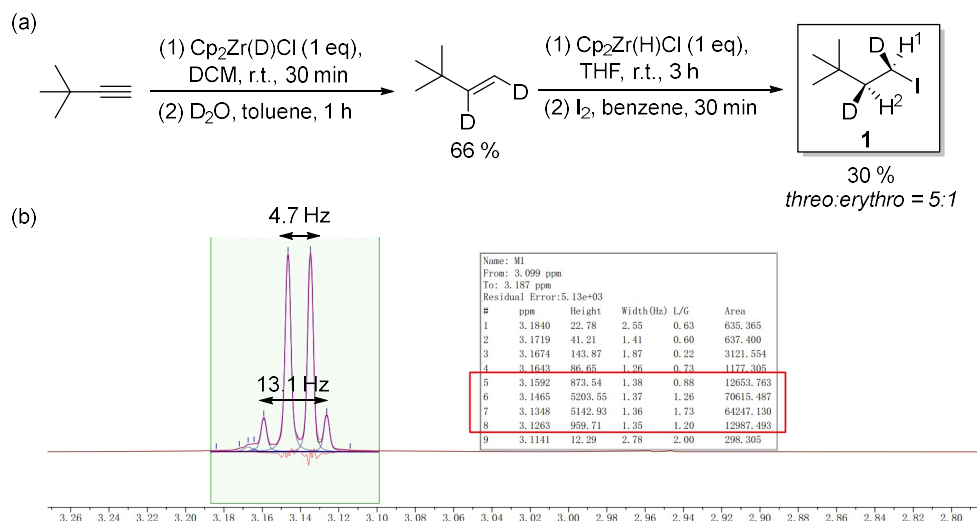


Figure S1. Synthesis and characterization of *t*-Bu substituted stereochemical probe **1**

During the process of repeating this synthetic method, we noticed that the magnitude of deuterium ratio can affect the results of $^1\text{H}\{^2\text{H}\}$ NMR simulation (Figure S2). We suggested that this uncertainty was mainly caused by the peak overlapping between the desired, dideuterated stereochemical probe **1** and its monodeuterated derivative. However, consistent simulation results can still be obtained by analyzing the region of 1.85-1.91 ppm (H^2 of compound **1**) in ^1H NMR spectra. Thus confirmed the reproducibility of this method.

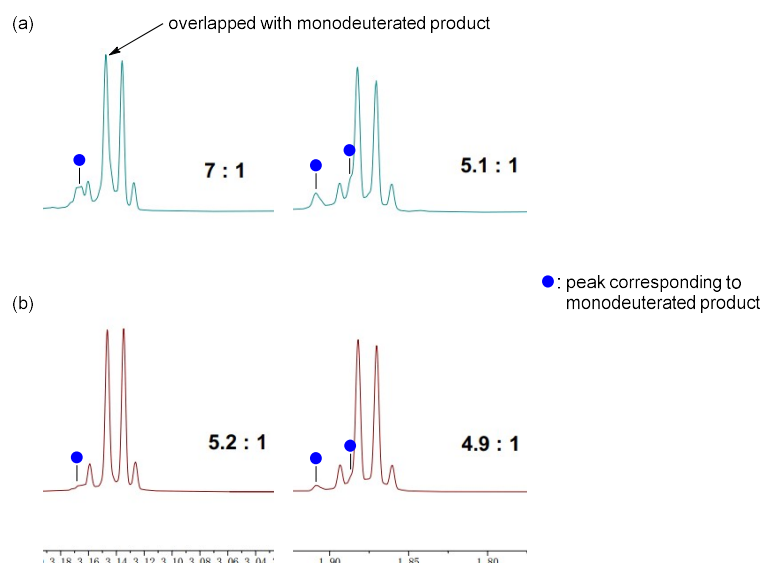


Figure S2. Influence of the deuterium ratio on simulation results: (a) Synthesized stereochemical probe **1** with relative low deuterium ratio; peak overlapping between stereochemical probe **1** and its monodeuterated derivative caused simulation error (b) Synthesized stereochemical probe **1** with high deuterium ratio

2.2 TBS Protected Stereochemical Probe 2

To unambiguously determine the relationship between the magnitude of H_1 - H_2 coupling constant and the relative configuration of compound **2**, various synthetic routes were carried out to independently synthesize this TBS protected stereochemical probe. Procedures of these synthetic routes were summarized in Figure S3.

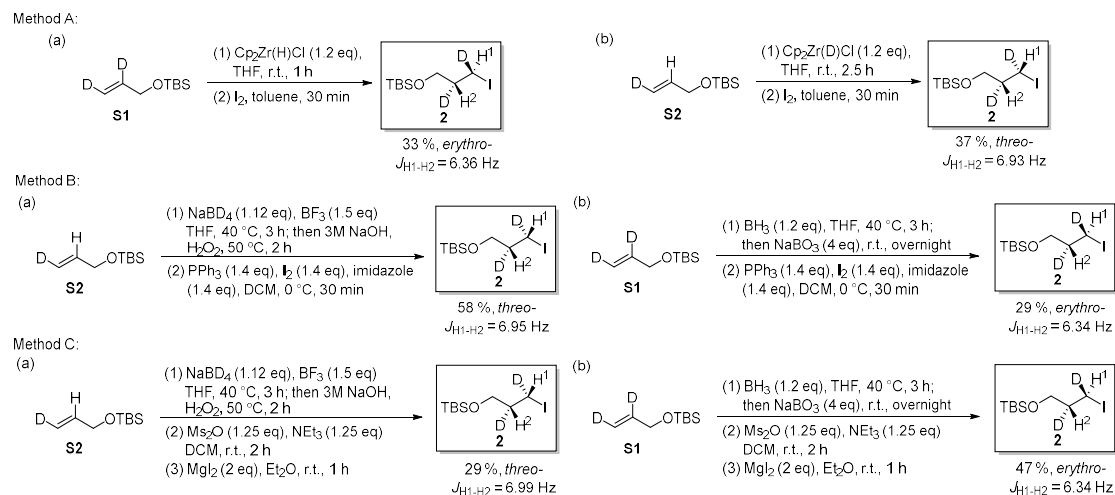


Figure S3. Summarization of the synthetic methods that leading to TBS protected stereochemical probe **2**

One thing noticeable is that the H^1 - H^2 coupling constant of the *threo*-isomer of compound **2** is larger than its *erythro*-isomer, while in the case of *t*-Bu substituted stereochemical probe **1**, the *erythro*-isomer is the larger one. We suggest that these two stereochemical probe **1** and **2** may adopt different conformation, thus caused this seemingly contradiction (Figure S4). *t*-Bu substituted stereochemical

probe **1** mainly adopts the *anti* conformation due to the large steric hindrance of the bulky *t*-Bu group. However, TBS protected stereochemical probe **2** may adopt the *gauche* conformation as the CH₂OTBS group is less sterically encumbered. Hyperconjugation effect ($\sigma_{C-H}/\sigma_{C-D} \rightarrow \sigma^*_{C-I}$) may also favored the *gauche* conformer of compound **2**.

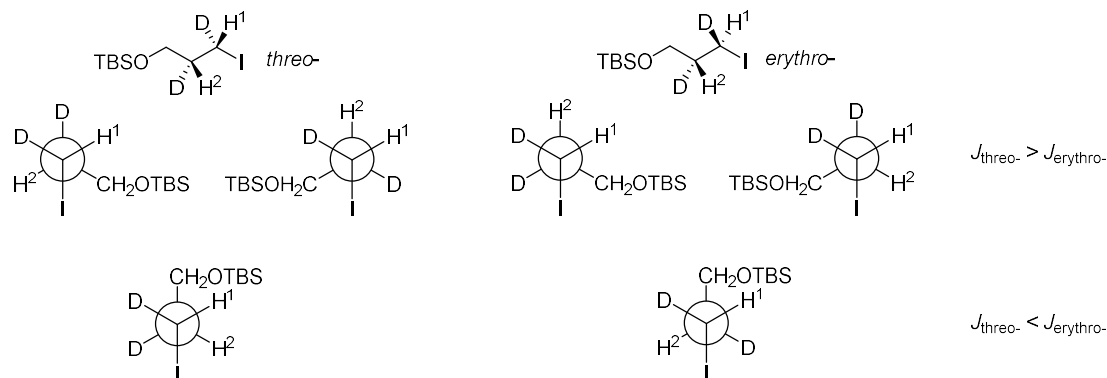


Figure S4. The relationship between the magnitude of H¹-H² coupling constant and the conformation of compound **2**

Method A: This reaction was carried out by a slightly modified procedure of Gladysz *et al.*¹ A dry Schlenk flask was charged with Cp₂Zr(H)Cl (495 mg, 1.9 mmol, 1.2 eq) and a stir bar. THF (10 mL) and **S1** (278 mg, 1.6 mmol, 1 eq) was added stepwise under the protection of argon. After stirring the reaction mixture at r.t. for 1-2.5 h, THF solvent was removed in vacuo. Toluene (10 mL) was then added to redissolve the solid residue. The resulted solution was cooled to 0 °C and a solution of iodine in toluene (406 mg I₂ in 2 mL toluene) was added. The mixture was stirred for 30 min at 0 °C and then saturated Na₂S₂O₃ solution was added to quench the reaction mixture. The aqueous phase was extracted with Et₂O after filtering through a short pad of celite. The combined organic phase was washed with brine, dried over Na₂SO₄, and concentrated in vacuo. The resulting residue was further purified by flash column chromatography (eluted with petroleum ether/ethyl acetate 20 : 1) to afford the desired product **2** (*erythro*-isomer, 131 mg, 33 % yield). When using Cp₂Zr(D)Cl and **S2** as substrates, the *threo*-isomer of compound **2** can be obtained in 33 % isolated yield.

Method B: The first step of this method was carried out by a slightly modified procedure of Kambe *et al.*⁹ To THF suspension (11 mL) of NaBD₄ (497 mg, 11.9 mmol, 1.12 eq) and **S2** (1.84 g, 10.6 mmol, 1 eq) was added BF₃•Et₂O (2.26 g, 15.9 mmol, 1.5 eq) was at 25 °C over 20 min. The resulting suspension was heated to 40 °C and stirred for 3 h. The reaction mixture was then cooled to 0 °C, and water (3.5 mL) was added dropwise cautiously, followed by 3 M NaOH (4.0 mL), and then 30% hydrogen peroxide (4.0 mL; dropwise). The resulting reaction mixture heated to 50 °C for 2 h. NaCl was then added to the reaction mixture and the aqueous phase was extracted with ether, washed with brine, and dried over Na₂SO₄. The solvent was removed, and the residue was then filtered through a short column of silica gel (eluted with petroleum ether/ethyl acetate 10:1). The resulting crude product was directly used in next step without further purification.

PPh₃ (38.1 mg, 0.14 mmol, 1.4 eq) and DCM (0.5 mL) was charged into a 5 mL sample flask and then cooled to 0 °C. I₂ (47.8 mg, 0.14 mmol, 1.4 eq) was added portionwise and stirred for 10 min.

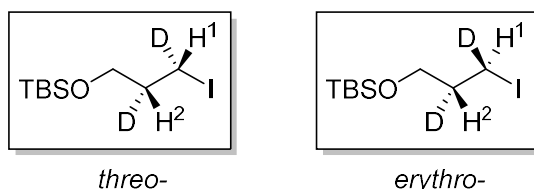
Crude product of first step (26 mg, ca. 0.1 mmol, 1 eq) was slowly added and stirred for further 30 min. After reaction completed, excess $\text{Na}_2\text{S}_2\text{O}_3$ was added to quench the reaction mixture and the aqueous phase was extracted by Et_2O . The combined organic phase was washed by brine, dried by Na_2SO_4 , and concentrated in vacuo. The resulting residue was further purified by flash column chromatography (eluted with petroleum ether/ethyl acetate 20:1) to afford the desired product **2** (*threo*-isomer, 29.6 mg, 58 % yield).

Modified procedure of this method can be carried out to synthesize the *erythro*-isomer of compound **2**: **S1** (1.07 g, 6.1 mmol, 1 eq) and 1 mol/L $\text{BH}_3\cdot\text{THF}$ (7.35 mL, 7.4 mmol, 1.2 eq) was added stepwise to a argon filled, dry Schlenk flask. The resulting solution was heated to 40 °C and stirred for 3 h. The reaction mixture was then cooled to 0 °C, and water (4 mL) was added drop wise cautiously, followed by $\text{NaBO}_3\cdot 4\text{H}_2\text{O}$ (5.8 g, 37.6 mmol, 6.2 eq). The resulting reaction mixture was then warmed to r.t. and stirred overnight. Workup and subsequent experimental manipulation is consistent with the procedure described above.

Method C: The first step of this method is consistent with method B. The crude product of first step (ca. 2 mmol, 1 eq) was dissolved in DCM (8 mL). NEt_3 (253 mg, 2.5 mmol, 1.25 eq) was added, followed by portionwise addition of Ms_2O (436 mg, 2.5 mmol, 1.25 eq) at 0 °C. The resulting reaction mixture was then naturally warmed to r.t. and stirred for 2 h. Saturated NaHCO_3 solution (40 mL) was then added to the reaction mixture and the aqueous phase was extracted with ether, washed with brine, and dried over NaSO_4 . The solvent was removed, and the residue was then filtered through a short column of silica gel (eluted with petroleum ether/ethyl acetate 10:1). The resulting crude product was directly used in next step without further purification.

This reaction was carried out by a slightly modified procedure of Madonik *et al.*¹⁰ The crude product of previous step (ca. 1.2 mmol, 1 eq) was transferred into a round bottom flask with a precharged stir bar. Freshly prepared Et_2O solution of MgI_2 (0.2 mol/L, 12 mL, 2.4 mmol, 2 eq) was added under stirring and then allowed to stir for further 1 h at r.t. After reaction completed, excess $\text{Na}_2\text{S}_2\text{O}_3$ was added to quench the reaction mixture and the aqueous phase was extracted by Et_2O . The combined organic phase was washed by brine, dried by Na_2SO_4 , and concentrated in vacuo. The resulting residue was further purified by flash column chromatography (eluted with petroleum ether/diethyl ether 30 : 1) to afford the desired product **2** (*threo*-isomer, 297 mg, 29 % yield). The *erythro*-isomer of compound **2** can be obtained by this method when use **S2** as substrate.

Characterization data of compound **2**:



$^1\text{H}\{^2\text{H}\}$ NMR (400 MHz, CDCl_3) δ *threo*-isomer: 3.66 (d, $J = 5.7$ Hz, 2H), 3.26 (d, $J = 7.0$ Hz, 1H), 1.97 (dt, $J = 7.1, 5.7$ Hz, 1H), 0.90 (s, 9H), 0.07 (s, 6H); *erythro*-isomer: 3.66 (d, $J = 5.7$ Hz, 2H), 3.26 (d, $J = 6.3$ Hz, 1H), 1.97 (q, $J = 7.9$ Hz, 1H), 0.90 (s, 9H), 0.07 (s, 6H).

^{13}C NMR (101 MHz, CD_2Cl_2) δ *threo*-isomer: 62.3, 35.8 (t, $J = 19.7$ Hz), 25.6, 18.1, 3.6 (t, $J = 23.3$ Hz), -5.7; *erythro*-isomer: 62.3, 35.8 (t, $J = 19.7$ Hz), 25.6, 18.1, 3.6 (t, $J = 23.2$ Hz), -5.7.

IR (ATR): *threo*-isomer: 2955, 2929, 2857, 1472, 1252, 1747, 1098, 1005, 936, 833, 773 cm^{-1} ; *erythro*-isomer: 2954, 2929, 2857, 1471, 1255, 1099, 1006, 940, 879, 835, 776 cm^{-1} .

HRMS (APCI) calcd. for $\text{C}_9\text{H}_{20}\text{D}_2\text{IOSi}^+ [\text{M}+\text{H}^+]$ 303.0605; found *threo*-isomer: 303.0597; *erythro*-isomer: 303.0603.

2.3 Epimerization of Stereochemical Probes

Our preliminary stereochemical investigations was carried out under standard Catellani reaction conditions and complete epimerization of recovered stereochemical probe was observed (Figure S5):

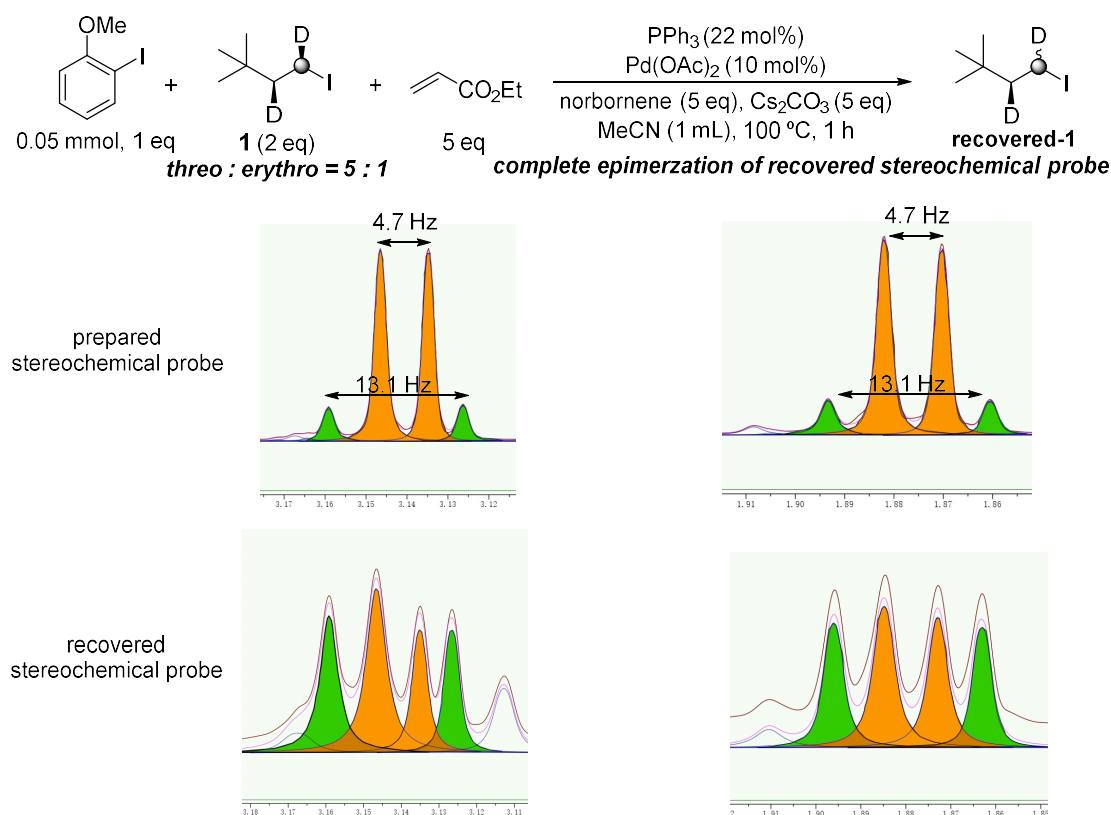
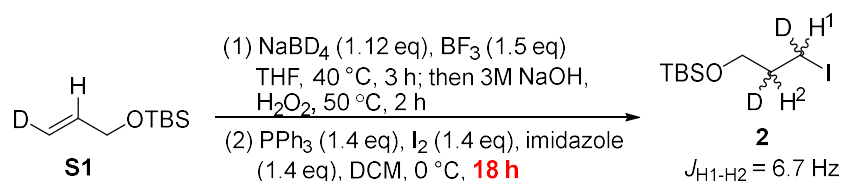


Figure S5. Epimerization of *t*-Bu substituted stereochemical probe **1** under standard Catellani reaction conditions

Similar epimerization process was also observed during the synthesis of TBS protected stereochemical probe **2** by extending the reaction time:



We suggest that these epimerization processes were caused by the in situ formed free iodine anion during the reaction progress.¹¹ Further control experiments confirmed this hypothesis (Figure S6):

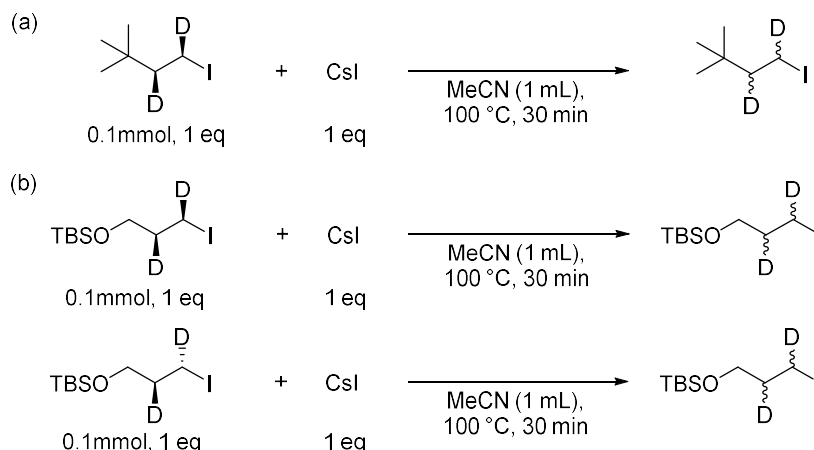


Figure S6. Epimerization of stereochemical probes in the presence of free iodine anion

Based on the results discussed above, we planned to do the study by performing stoichiometric reactions between the synthesized palladacycles and the probe molecules. Meanwhile, in order to eliminate the affection of the iodide anion generated as a byproduct after alkyl substitution, silver salts should be used as an iodide trapper. As shown in Figure S7, this epimerization process can indeed be suppressed by increasing the amount of Ag_2CO_3 base and carefully controlling the reaction time.

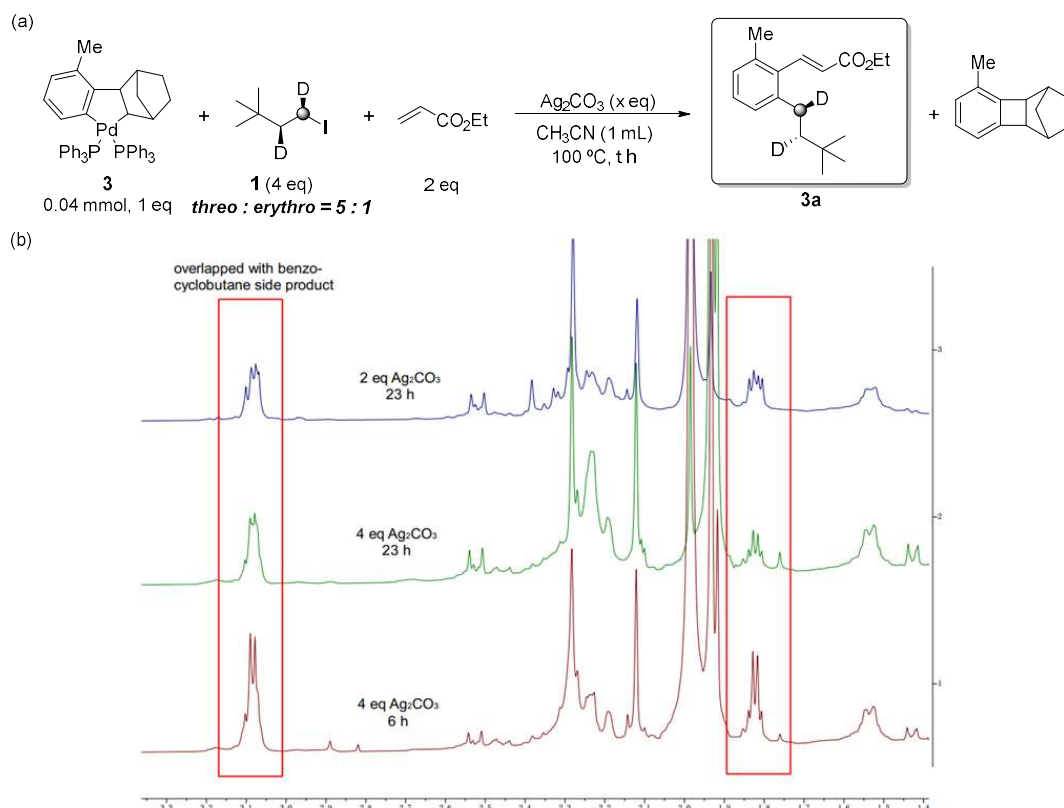
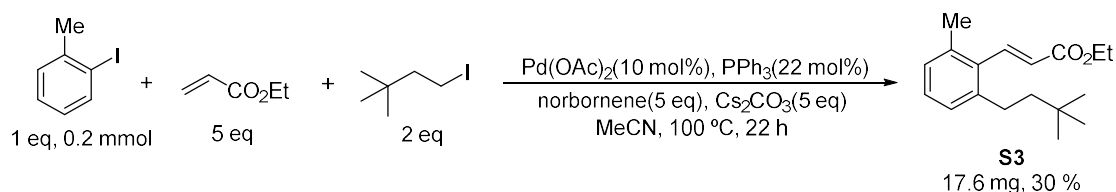


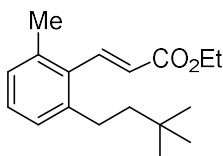
Figure S7. Suppressing the epimerization process by adding Ag_2CO_3 as base and reducing the reaction time (peaks corresponding to unreacted stereochemical probe was highlighted)

3. Undeuterated Alkylation Product Synthesis



An oven-dried 15 mL vial was charged with Pd(OAc)₂ (4.48 mg, 0.02 mmol, 0.1 eq), PPh₃ (11.5 mg, 0.044 mmol, 0.22 eq), and Cs₂CO₃ (325.8 mg, 1.0 mmol, 5 eq). Then evacuated and backfilled with argon (3 times). MeCN (2 mL), 1-iodo-2-methylbenzene (43.6 mg, 0.2 mmol, 1 eq), 3,3-dimethyl-1-iodobutane (84.8 mg, 0.4 mmol, 2 eq), ethyl acrylate (100 mg, 1.0 mmol, 5 eq) and norbornene (94.1 mg, 1.0 mmol, 5 eq) was added stepwise under the protection of argon atmosphere. The vial was then sealed with a PTFE screwed cap and stirred on a metal bath preheated to 100 °C for 22 hours. Then the reaction mixture was filtered through a short pad of celite to give a clear solution. The filtrate was concentrated in vacuo and the resulting residue was further purified by flash column chromatography (eluted with petroleum ether/ethyl acetate 100 : 1) to afford the desired product **S3** (17.6 mg, 30 % yield).

Characterization data of compound **S3** :

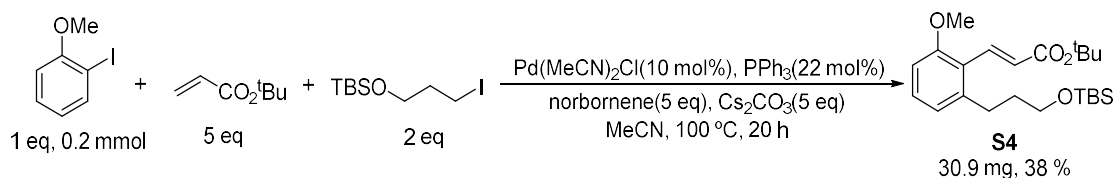


¹H NMR (400 MHz, CDCl₃) δ 7.86 (d, *J* = 16.4 Hz, 1H), 7.19 – 7.11 (m, 1H), 7.05 (d, *J* = 7.6 Hz, 2H), 6.06 (d, *J* = 16.4 Hz, 1H), 4.28 (q, *J* = 7.1 Hz, 2H), 2.64 – 2.55 (m, 2H), 2.34 (s, 3H), 1.44 – 1.37 (m, 2H), 1.34 (t, *J* = 7.1 Hz, 3H), 0.94 (s, 9H).

¹³C NMR (101 MHz, CDCl₃) δ 166.6, 143.3, 142.1, 136.3, 133.7, 128.3, 128.1, 127.2, 124.2, 60.5, 46.0, 30.7, 29.3, 29.2, 21.2, 14.3.

IR (ATR): 3064, 2954, 2868, 1717, 1640, 1465, 1365, 1303, 1263, 1189, 1165, 1036, 988, 766 cm⁻¹.

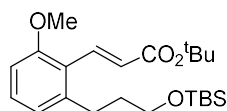
HRMS (ESI): calcd. for C₁₈H₂₆NaO₂⁺ [*M*+Na⁺] 297.1825; found 297.1814.



An oven-dried 15 mL vial was charged with Pd(MeCN)₂Cl₂ (5.19 mg, 0.02 mmol, 0.1 eq), PPh₃ (11.5 mg, 0.044 mmol, 0.22 eq), and Cs₂CO₃ (325.8 mg, 1.0 mmol, 5 eq). Then evacuated and backfilled with argon (3 times). MeCN (2 mL), 1-iodo-2-methoxybenzene (46.8 mg, 0.2 mmol, 1 eq), *tert*-butyl(3-iodopropoxy)dimethylsilane (120 mg, 0.4 mmol, 2 eq), *tert*-butyl acrylate (128 mg, 1.0 mmol, 5 eq) and norbornene (94.1 mg, 1.0 mmol, 5 eq) was added stepwise under the protection

of argon atmosphere. The vial was then sealed with a PTFE screwed cap and stirred on a metal bath preheated to 100 °C for 20 hours. Then the reaction mixture was filtered through a short pad of celite to give a clear solution. The filtrate was concentrated in vacuo and the resulting residue was further purified by flash column chromatography (eluted with petroleum ether/ethyl acetate 60 : 1) to afford the desired product **S4** (30.9 mg, 38 % yield).

Characterization data of compound **S4** :

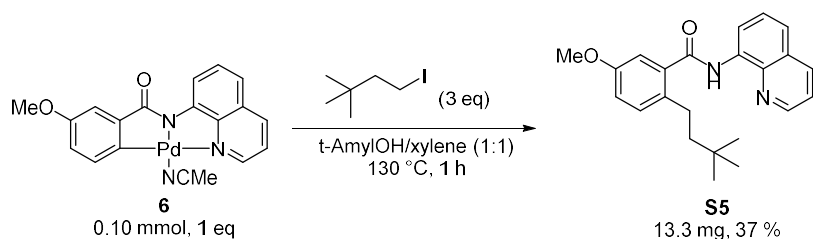


¹H NMR (400 MHz, CDCl₃) δ 7.79 (d, *J* = 16.1 Hz, 1H), 7.21 (t, *J* = 8.0 Hz, 1H), 6.84 (dd, *J* = 7.7, 1.1 Hz, 1H), 6.78 (d, *J* = 8.2 Hz, 1H), 6.58 (d, *J* = 16.1 Hz, 1H), 3.86 (s, 3H), 3.64 (t, *J* = 6.3 Hz, 2H), 2.85 – 2.76 (m, 2H), 1.86 – 1.75 (m, 2H), 1.53 (s, 9H), 0.90 (s, 9H), 0.05 (s, 6H).

¹³C NMR (101 MHz, CDCl₃) δ 167.3, 159.2, 143.9, 137.3, 129.7, 124.4, 122.4, 122.1, 108.8, 80.0, 62.4, 55.5, 34.2, 30.1, 28.3, 26.0, 18.3, -5.3.

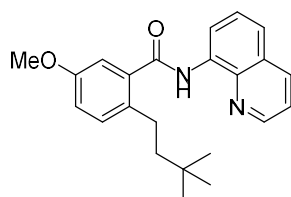
IR (ATR): 2929, 1705, 1625, 1595, 1573, 1470, 1390, 1366, 1311, 1254, 1157, 1087, 984, 834, 774, 754, 662 cm⁻¹.

HRMS (APCI): calcd. for C₂₃H₃₉O₄Si⁺ [M+H⁺] 407.2612; found 407.2628.



This reaction was carried out by a slightly modified procedure of Chen *et al.*⁵ In a argon-filled glovebox, an oven-dried 15 mL vial was charged with 8-aminoquinoline coordinated palladacycle complex **6** (48.4 mg, 0.10 mmol, 1 eq), *t*-AmylOH/xylene (1:1, 1 mL), 3,3-dimethyl-1-iodobutane (63.6 mg, 0.3 mmol, 3 eq) in a stepwise manner. The vial was then sealed with a PTFE screwed cap in the glovebox. The vial was subsequently taken out of the glovebox and stirred on a metal bath preheated to 130 °C for 1 hour. Then the reaction mixture was diluted with DCM and aqueous HI solution (55 %, 10 μL) was added to quench the reaction. After stirring at r.t. for 1 h, the reaction mixture was concentrated in vacuo and the resulting residue was further purified by flash column chromatography (eluted with petroleum ether/ethyl acetate 20:1 to 10:1) to afford the desired product **S5** (13.3 mg, 37 % yield).

Characterization data of compound **S5**:



^1H NMR (400 MHz, CDCl_3) δ 10.15 (s, 1H), 8.95 (dd, $J = 7.5, 1.5$ Hz, 1H), 8.78 (dd, $J = 4.3, 1.7$ Hz, 1H), 8.19 (dd, $J = 8.3, 1.7$ Hz, 1H), 7.64 – 7.58 (m, 1H), 7.56 (dd, $J = 8.3, 1.5$ Hz, 1H), 7.46 (dd, $J = 8.3, 4.2$ Hz, 1H), 7.23 (d, $J = 8.5$ Hz, 1H), 7.16 (d, $J = 2.8$ Hz, 1H), 6.97 (dd, $J = 8.5, 2.78$ Hz, 1H), 3.84 (s, 3H), 2.86 – 2.74 (m, 2H), 1.62-1.53 (m, 2H), 0.83 (s, 9H).

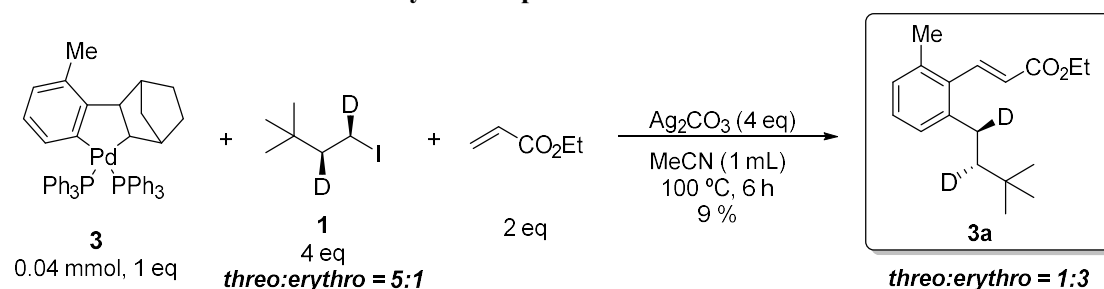
^{13}C NMR (101 MHz, CDCl_3) δ 168.2, 157.6, 148.2, 138.4, 137.6, 136.5, 134.7, 133.6, 131.5, 128.0, 127.5, 121.8, 121.7, 116.8, 116.2, 112.5, 55.5, 46.8, 30.6, 29.2, 28.0.

IR (ATR): 3351, 2953, 1677, 1608, 1522, 1483, 1424, 1385, 1326, 1288, 1099, 1042, 826, 791 cm^{-1} .

HRMS (ESI): calcd. for $\text{C}_{23}\text{H}_{27}\text{N}_2\text{O}_2^+$ $[\text{M}+\text{H}^+]$ 363.2067; found 363.2054.

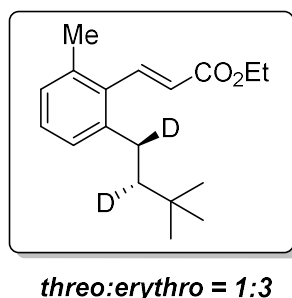
4. Stereochemical Investigations

4.1 Norbornene Derived Palladacycle Complex 3



In a argon-filled glovebox, an oven-dried 15 mL vial was charged with norbornene derived palladacycle complex **3** (32.6 mg, 0.04 mmol, 1 eq), MeCN (0.5 mL), *t*-Bu substituted stereochemical probe **1** (34.2 mg, 0.16 mmol, 4 eq), ethyl acrylate (8 mg, 0.08 mmol, 2 eq), MeCN (0.5 mL) and Ag_2CO_3 (44.1 mg, 0.16 mmol, 4 eq) in a stepwise manner. The vial was then sealed with a PTFE screwed cap in the glovebox. The vial was subsequently taken out of the glovebox and stirred on a metal bath preheated to 100 °C for 6 hours. Then the reaction mixture was filtered through PTFE Syringe Filter to give a clear solution. The filtrate was concentrated in vacuo and the resulting residue was further purified by flash column chromatography (eluted with petroleum ether/ethyl acetate 100 : 1) to afford the desired product **3a** (1.05 mg, 9 % yield).

Characterization data of compound **3a** :



$^1\text{H}\{^2\text{H}\}$ NMR (400 MHz, CDCl_3) δ 7.86 (d, J = 16.4 Hz, 1H), 7.15 (t, J = 7.5 Hz, 1H), 7.08 – 7.02 (m, 2H), 6.06 (d, J = 16.4 Hz, 1H), 4.28 (q, J = 7.1 Hz, 2H), 2.57 (d, *erythro*-isomer: J = 13.0 Hz; *threo*-isomer: J = 4.8 Hz, 1H), 2.34 (s, 3H), 1.40 – 1.31 (m, 4H), 0.94 (s, 9H).

HRMS (ESI): calcd. for $\text{C}_{18}\text{H}_{24}\text{D}_2\text{NaO}_2^+$ [$\text{M}+\text{Na}^+$] 299.1951; found 299.1942.

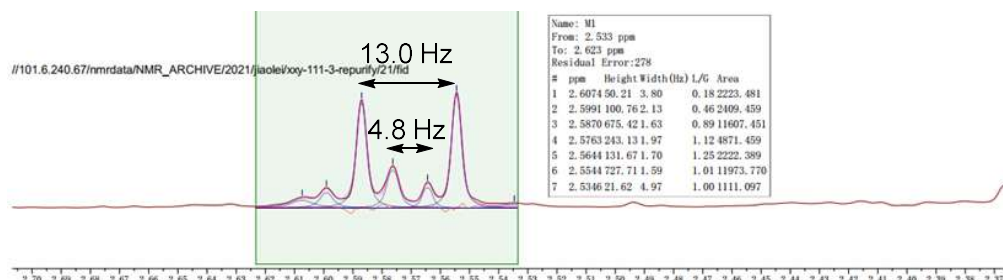
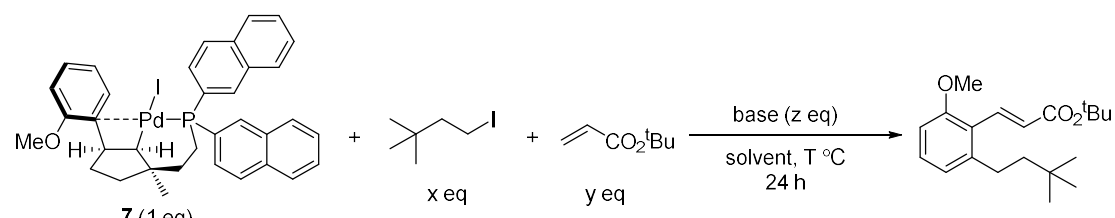


Figure S8. Determine the diastereomeric ratio of **3a** by NMR simulation

4.2 Alkene-ligand Derived Palladacycle Complex 4

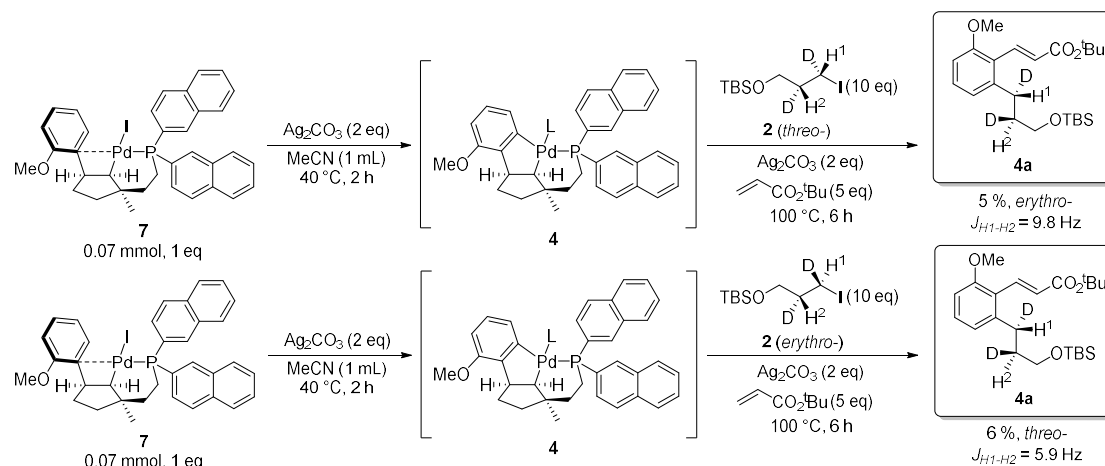
Our stereochemical investigations on the alkene-ligand derived palladacycle complex **4** (*in situ* formed by the reaction of its precursor **7** with base) was initiated by testing the reactivity of this complex with 1-iodo-3,3-dimethyl butane (undeuterated derivative of stereochemical probe **1**). However, no alkylation product formation was observed even we increased the amount of alkyl iodide to 30 eq (Figure S9).



	x	y	base	solvent, T	yield
1	4	4	Ag ₂ CO ₃ , 4 eq	MeCN, 100 °C	undetected
2	30	4	Ag ₂ CO ₃ , 4 eq	MeCN, 100 °C	undetected
3	20	10	Cs ₂ CO ₃ , 10 eq	MeCN, 100 °C	undetected
4	20	10	Ag ₂ CO ₃ , 4 eq	DMF, 120 °C	undetected

Figure S9. Test the reactivity of alkene-ligand derived palladacycle complex **4**

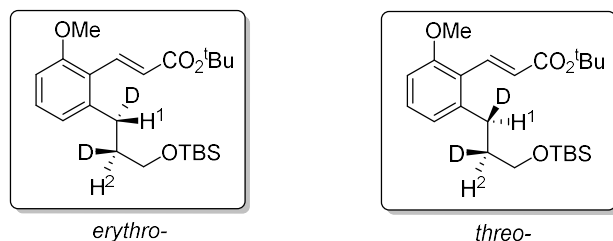
Thus, subsequent stereochemical investigations were carried out with less sterically encumbered, TBS protected stereochemical probe **2**:



In an argon-filled glovebox, an oven-dried 15 mL vial was charged with complex **7** (51.4 mg, 0.07 mmol, 1 eq), Ag₂CO₃ (38.6 mg, 0.14 mmol, 2 eq) and MeCN (1 mL) in a stepwise manner. The vial was then sealed with a PTFE screwed cap in the glovebox. The vial was subsequently taken out of the glovebox and stirred on a metal bath preheated to 40 °C for 2 hours. Then the reaction mixture was added Ag₂CO₃ (38.6 mg, 0.14 mmol, 2 eq), TBS protected stereochemical probe **2** (211 mg, 0.7 mmol, 10 eq) and *tert*-butyl acrylate (44.8 mg, 0.35 mmol, 5 eq) in glove box. After stirring at 100 °C for 6 hours, the reaction mixture was filtered through a short pad of celite to give a clear solution. The filtrate was concentrated in vacuo and the resulting residue was purified by flash column chromatography (eluted with petroleum ether/ethyl acetate 60:1). Further purification was

carried out by preparative HPLC to afford the desired product **4a** (contaminated with inseparable carbonate ester impurity, 1.5-1.7 mg, 5-6 % yield).

Characterization data of compound **4a** :



$^1\text{H}\{^2\text{H}\}$ NMR (400 MHz, CDCl_3) δ *erythro*-isomer: 7.79 (d, $J = 16.2$ Hz, 1H), 7.24 – 7.17 (m, 1H), 6.84 (dd, $J = 7.6, 1.1$ Hz, 1H), 6.80 – 6.76 (m, 1H), 6.59 (d, $J = 16.1$ Hz, 1H), 3.86 (s, 3H), 3.63 (d, $J = 6.3$ Hz, 2H), 2.78 (d, $J = 9.8$ Hz, 1H), 1.79 – 1.75 (m, 1H), 1.53 (s, 9H), 0.90 (s, 9H), 0.05 (s, 6H); *threo*-isomer: 7.79 (d, $J = 16.1$ Hz, 1H), 7.20 (t, $J = 8.0$ Hz, 1H), 6.84 (dd, $J = 7.6, 1.1$ Hz, 1H), 6.78 (d, $J = 8.2$ Hz, 1H), 6.58 (d, $J = 16.1$ Hz, 1H), 3.86 (s, 3H), 3.63 (d, $J = 6.3$ Hz, 2H), 2.78 (d, $J = 5.9$ Hz, 1H), 1.77 (q, $J = 6.5$ Hz, 1H), 1.53 (s, 9H), 0.90 (s, 9H), 0.05 (s, 6H).

HRMS (APCI): calcd. for $\text{C}_{23}\text{H}_{37}\text{D}_2\text{O}_4\text{Si}^+ [\text{M}+\text{H}^+]$ 409.2738; found 409.2732.

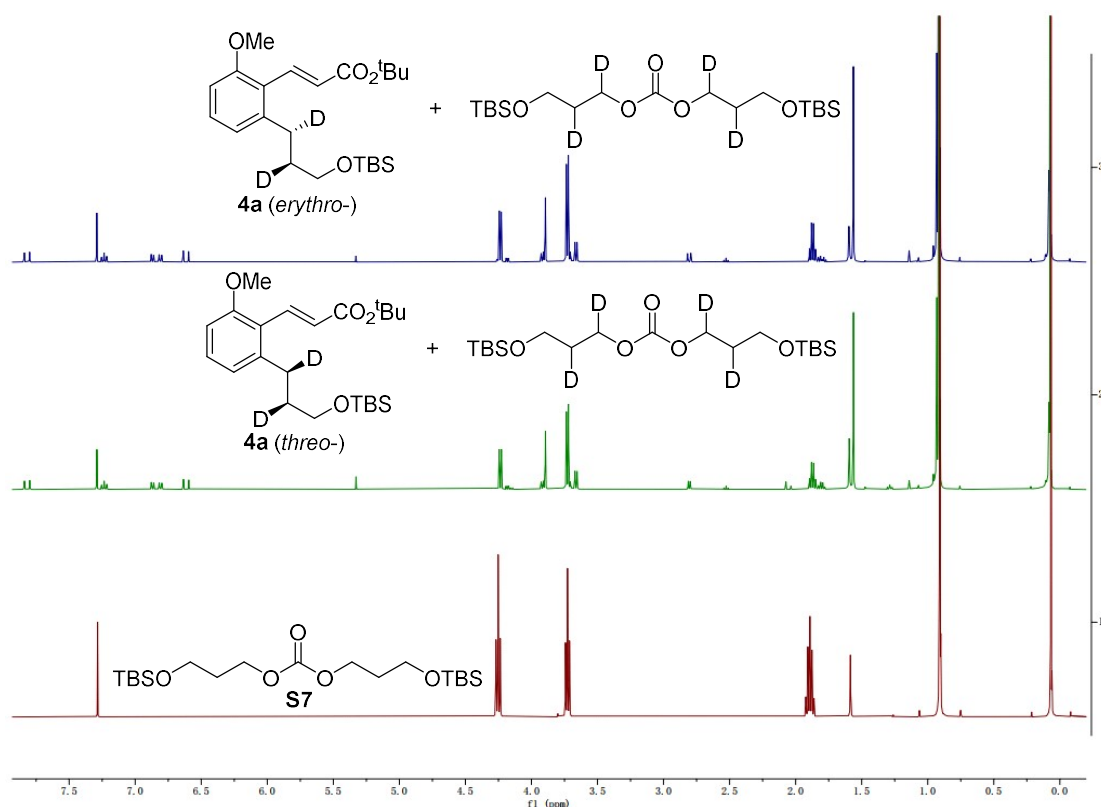
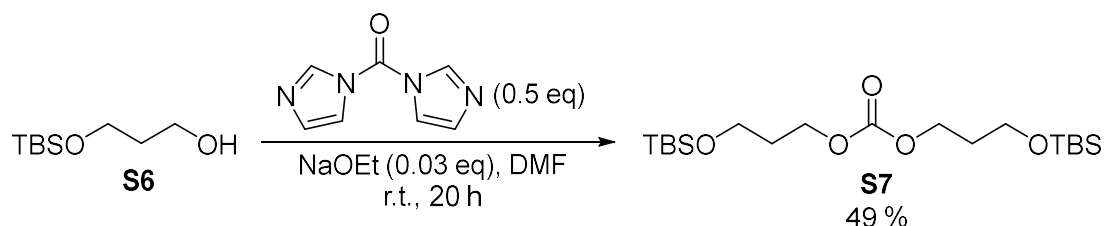


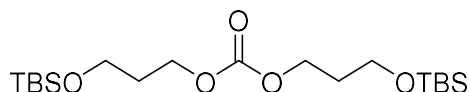
Figure S10. Assignment of the carbonate ester impurity

Carbonate ester **S7** was synthesized as following:¹²



A flame-dried flask was charged with CDI (405 mg, 2.5 mmol, 0.53 eq), 3-((tert-butyldimethylsilyl)oxy)propan-1-ol (905 mL, 4.7 mmol, 1 eq), and DMF (3 mL) and this mixture was treated with EtONa (10.2 mg, 0.15 mmol, 0.03 eq) and stirred at r.t. for 20 h. The mixture was then poured into sat. aq. NH_4Cl and extracted with Et_2O . The combined organic layers were then washed with brine, dried over Na_2SO_4 , filtered, and concentrated in vacuo. The resulting residue was further purified by flash column chromatography (eluted with petroleum ether/ethyl acetate 10 : 1) to afford the desired product **S7** (464 mg, 49 % yield).

Characterization data of compound **S7** :



^1H NMR (400 MHz, CDCl_3) δ 4.25 (t, $J = 6.4$ Hz, 4H), 3.73 (t, $J = 6.0$ Hz, 4H), 1.89 (p, $J = 6.2$ Hz, 4H), 0.91 (s, 18H), 0.07 (s, 12H).

^{13}C NMR (101 MHz, CDCl_3) δ 155.3, 64.9, 59.2, 31.8, 25.9, 18.3, -5.4.

IR (ATR): 2955, 2929, 2857, 1747, 1472, 1402, 1361, 1327, 1252, 1098, 1005, 936, 833, 773, 662 cm^{-1} .

HRMS (ESI): calcd. for $\text{C}_{19}\text{H}_{43}\text{O}_5\text{Si}_2^+$ $[\text{M}+\text{H}^+]$ 407.2644 found 407.2644.

The relationship between the magnitude of $\text{H}_1\text{-H}_2$ coupling constant and the relative configuration of compound **5a** was assigned based on the previous investigation of Biscoe *et al.* (Figure S11):¹³

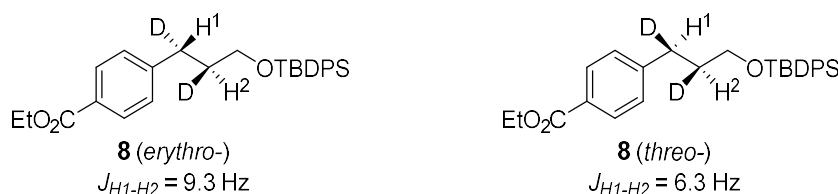


Figure S11. Assignment of the relationship between the magnitude of $\text{H}_1\text{-H}_2$ coupling constant and the relative configuration of compound **8** (which have similar structure with **4a**) by Biscoe *et al.*

A standard sample of **4a** with mixed *erythro*- and *threo*- isomer was also synthesized under standard Catellani conditions (Figure S12a). Our assignment result was further confirmed by comparing the $^1\text{H}\{^2\text{H}\}$ NMR spectra of this standard sample with *erythro*-/*threo*- isomer (Figure S12b).

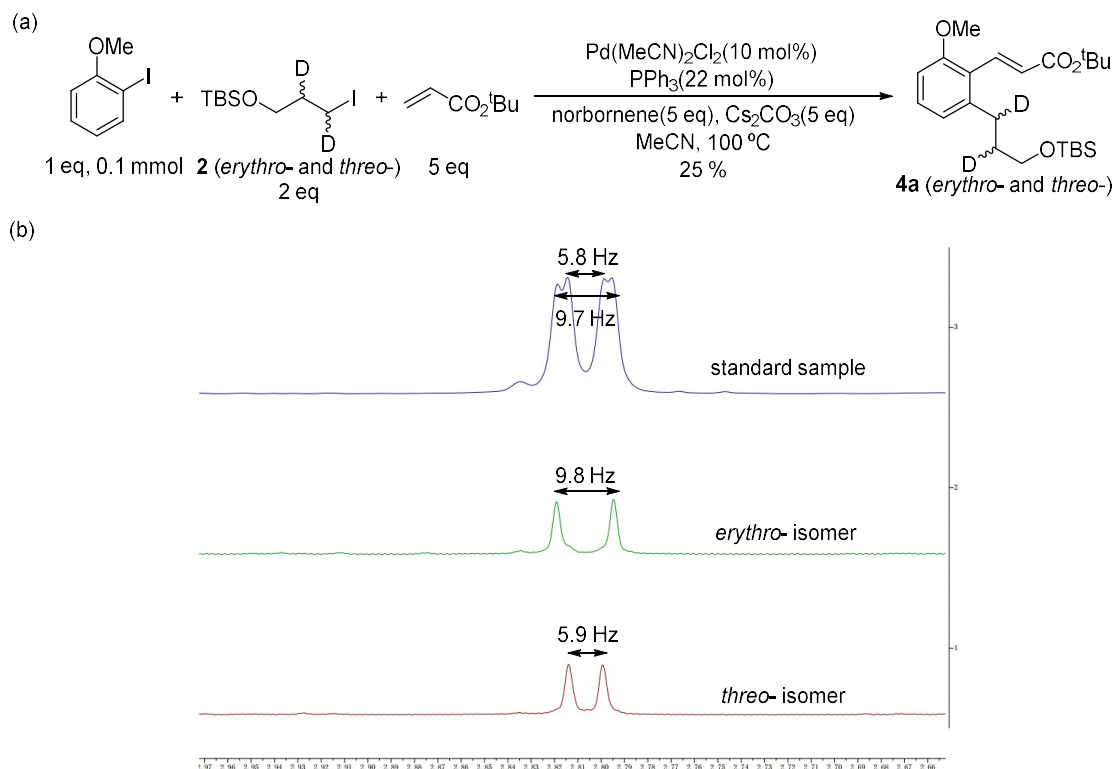


Figure S12. (a) Standard sample synthesis (b) Comparison between the ^1H NMR spectra of standard sample and *erythro*-/*threo*- isomer (no apodization function was used in NMR spectra processing to enhance the resolution)

To avoid the contamination of inseparable carbonate ester impurity, a step by step alkylation procedure was also tested (Figure S13a). After the *in situ* formation of palladacycle complex **4**, unreacted Ag_2CO_3 was removed by filtering through a PTFE Syringe Filter. TBSO protected stereochemical probe **2** was then introduced. After stirring the reaction mixture at 100 °C for 8 h, unreacted stereochemical probe **2** was removed by filtering through a short column of silica gel, and the remaining residue was further treated with acrylate and Cs_2CO_3 to give the desired alkylation product **4a**. However, a diminished diastereomeric ratio of the alkylation product was observed in this case (Figure S13b), presumably due to the rapid epimerization of stereochemical probe in the absence of silver salts.

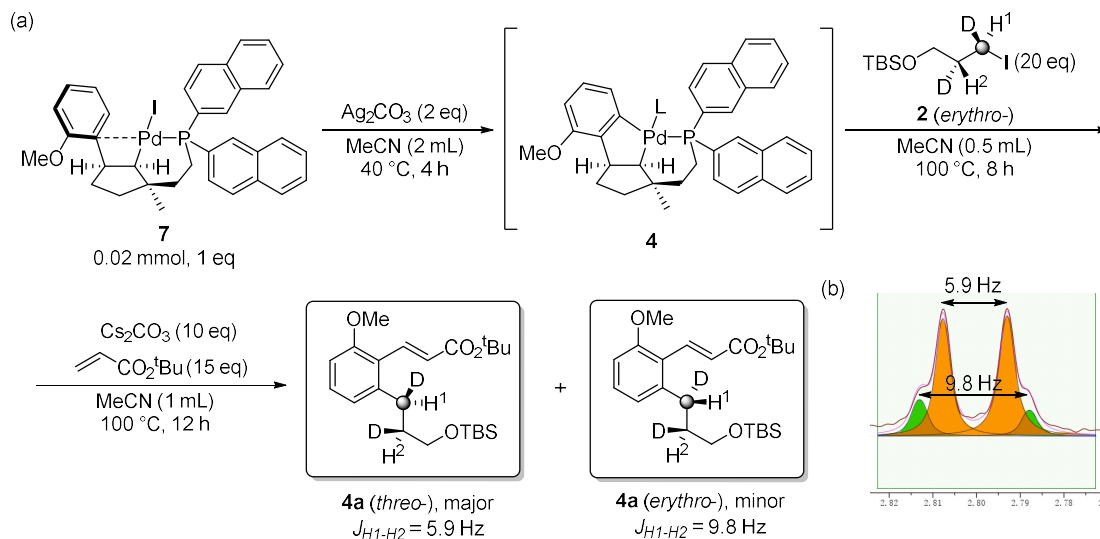
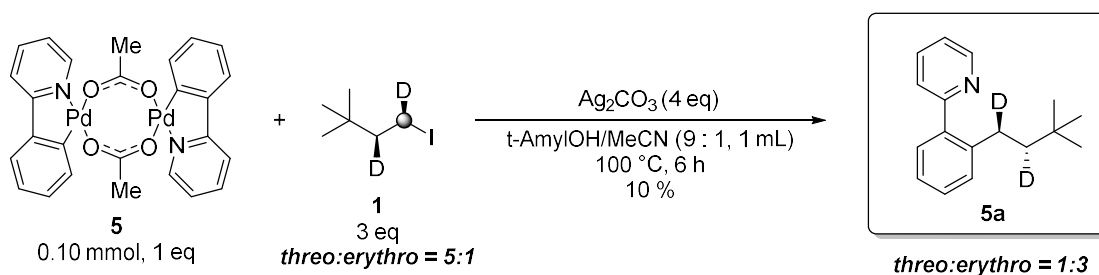


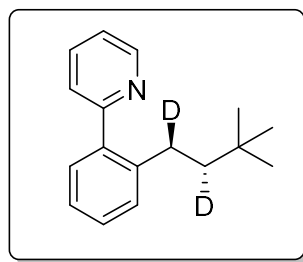
Figure S13. Erosion of product diastereomeric ratio in the absence of Ag_2CO_3

4.3 Pyridine Coordinated Palladacycle Complex **5**



This reaction was carried out by a slightly modified procedure of Zhang *et al.*⁴ In a argon-filled glovebox, an oven-dried 15 mL vial was charged with pyridine coordinated palladacycle complex **5** (48.4 mg, 0.10 mmol, 1 eq), *t*-AmylOH/MeCN (9:1, 1 mL), *t*-Bu substituted stereochemical probe **1** (64.2 mg, 0.3 mmol, 3 eq), Ag_2CO_3 (110 mg, 0.4 mmol, 4 eq) in a stepwise manner. The vial was then sealed with a PTFE screwed cap in the glovebox. The vial was subsequently taken out of the glovebox and stirred on a metal bath preheated to 100 °C for 6 hours. After the reaction was completed, the reaction mixture was allowed to cool down to room temperature. The reaction mixture was diluted with ethyl acetate and washed with aqueous Na_2S solution and brine, then filtered through a small pad of Celite. The filtrate was concentrated in vacuo. The resulting residue was further purified by PTLC separation (petroleum ether/ethyl acetate 7:1) to afford the desired product **5a** (4.8 mg, 10 % yield).

Characterization data of compound **5a** (undeuterated derivative of this compound is known):



threo:erythro = 1:3

$^1\text{H}\{^2\text{H}\}$ NMR (400 MHz, CDCl_3) δ 8.76 – 8.66 (m, 1H), 7.86 – 7.73 (m, 1H), 7.43 (d, $J = 7.8$ Hz, 1H), 7.37 – 7.25 (m, 5H), 2.62 (d, *erythro*-isomer: $J = 13.0$ Hz; *threo*-isomer: $J = 4.6$ Hz, 1H), 1.28 (d, *erythro*-isomer: $J = 13.0$ Hz; *threo*-isomer: $J = 4.6$ Hz, 1H), 0.75 (s, 9H).

HRMS (ESI): calcd. for $\text{C}_{17}\text{H}_{20}\text{D}_2\text{N}^+ [\text{M}+\text{H}^+]$ 242.1872; found 242.1866

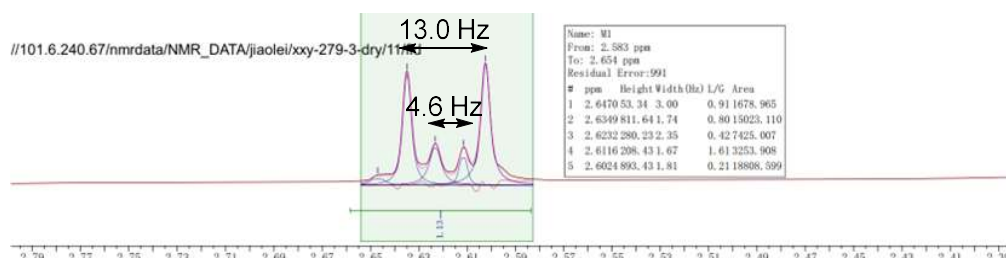
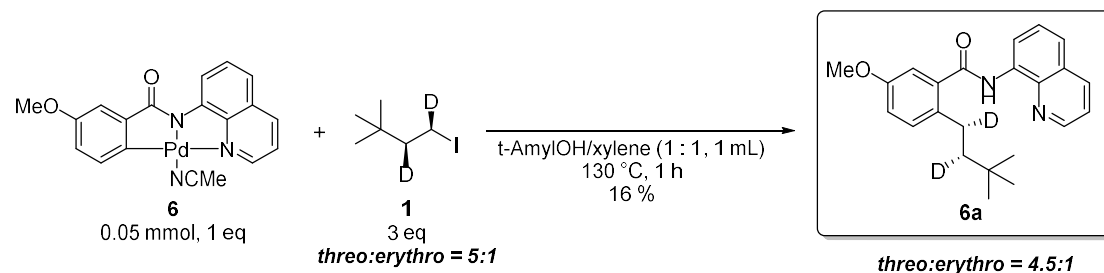


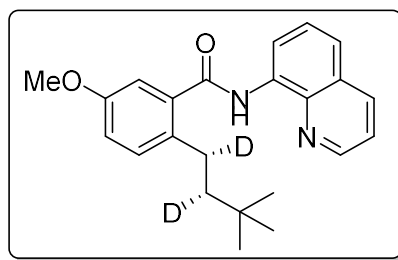
Figure S14. Determine the diastereomeric ratio of **5a** by NMR simulation

4.4 8-aminoquinoline Coordinated Palladacycle Complex **6**



This reaction was carried out by a slightly modified procedure of Chen *et al.*⁵ In a argon-filled glovebox, an oven-dried 15 mL vial was charged with 8-aminoquinoline coordinated palladacycle complex **6** (24.2 mg, 0.05 mmol, 1 eq), *t*-AmylOH/xylene (1:1, 1 mL), *t*-Bu substituted stereochemical probe **1** (32.1 mg, 0.15 mmol, 3 eq) in a stepwise manner. The vial was then sealed with a PTFE screwed cap in the glovebox. The vial was subsequently taken out of the glovebox and stirred on a metal bath preheated to 130 °C for 1 hour. Then the reaction mixture was diluted with DCM and aqueous HI solution (55 %, 5 μL) was added to quench the reaction. After stirring at r.t. for 1 h, the reaction mixture was concentrated in vacuo and the resulting residue was further purified by flash column chromatography (eluted with petroleum ether/ethyl acetate 20:1 to 10:1) to afford the desired product **6a** (3.3 mg, 16 % yield).

Characterization data of compound **6a**:



***threo:erythro* = 4.5:1**

$^1\text{H}\{^2\text{H}\}$ NMR (400 MHz, CDCl_3) δ 10.16 (s, 1H), 8.95 (d, J = 7.4 Hz, 1H), 8.78 (dd, J = 4.4, 1.6 Hz, 1H), 8.21 (dd, J = 8.3, 1.7 Hz, 1H), 7.62 (t, J = 7.9 Hz, 1H), 7.57 (dd, J = 8.3, 1.5 Hz, 1H), 7.47 (dd, J = 8.3, 4.2 Hz, 1H), 7.23 (d, J = 8.5 Hz, 1H), 7.16 (d, J = 2.7 Hz, 1H), 6.97 (dd, J = 8.5, 2.8 Hz, 1H), 3.85 (s, 3H), 2.76 (d, *erythro*-isomer: J = 13.0 Hz; *threo*-isomer: J = 4.7 Hz, 1H), 1.53 (d, overlapped with H_2O , *erythro*-isomer: J = 12.9 Hz; *threo*-isomer: J = 4.6 Hz, 1H), 0.83 (s, 9H).

HRMS (ESI): calcd. for $\text{C}_{23}\text{H}_{25}\text{D}_2\text{N}_2\text{O}_2^+$ [$\text{M}+\text{H}^+$] 365.2193; found 365.2179.

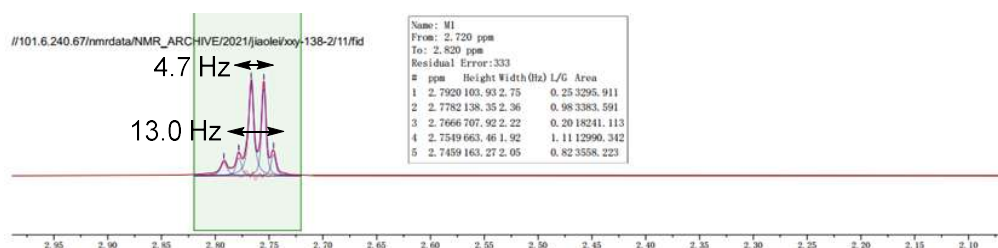


Figure S15. Determine the diastereomeric ratio of **7a** by NMR simulation

When this reaction was carried out in DMF solvent, stereoretentive alkylation product was still favored, albeit with a lower diastereomeric ratio (Figure S15, *threo:erythro* = 1.5:1):

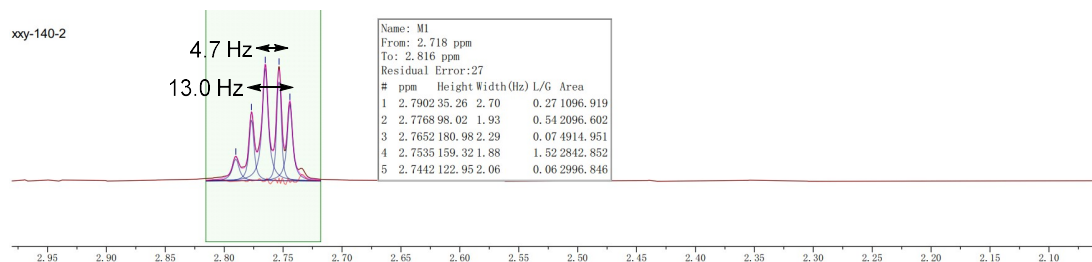


Figure S16. Determine the diastereomeric ratio of **7a** (formed in DMF solvent) by NMR simulation

5. DFT Calculations

5.1 Computational Methods

All of the quantum chemical calculations in this work were performed with Gaussian 16 program.¹⁴ Single point energy calculations and geometry optimization were carried out at M06-SMD(solvent)/SDD-6-311++G(d,p)//B3LYP-D3(BJ)-SMD(solvent)/Lan2ldz-6-31G(d) level of theory.¹⁵⁻²² To mimic the real reaction conditions, solvent = MeCN was selected for the alkylation transition states of complex **3** and **4'**; $\epsilon = 17.61$, $\epsilon_{\text{inf}} = 1.95$ was selected to mimic the *t*-AmylOH/MeCN for the alkylation transition states of complex **5**;²³ solvent = DMF was selected for the alkylation transition states of complex **6'**. Several important conformations were evaluated manually. Frequency calculations (298.15K, ideal gas) were also performed to evaluate the nature of optimized structures. For transition states with one imaginary frequency, IRC calculations were also carried out to confirm its connectivity between corresponding substrates and products. Nature population analysis was performed at M06-SMD(solvent)/SDD-6-311++G(d,p) level of theory by Gaussian 16 program.²⁴ Charge decomposition analysis (CDA)²⁵ was carried out at the B3LYP-D3(BJ)-SMD(solvent)/SDD-6-311G(d,p) level of theory by Multiwfn program²⁶. Energy levels of Kohn-Sham canonical molecular orbitals were calculated at the same level of theory. Visualizations were completed through CYLview and Multiwfn program.²⁷

5.2 Geometry Structures of Alkylation Transition States

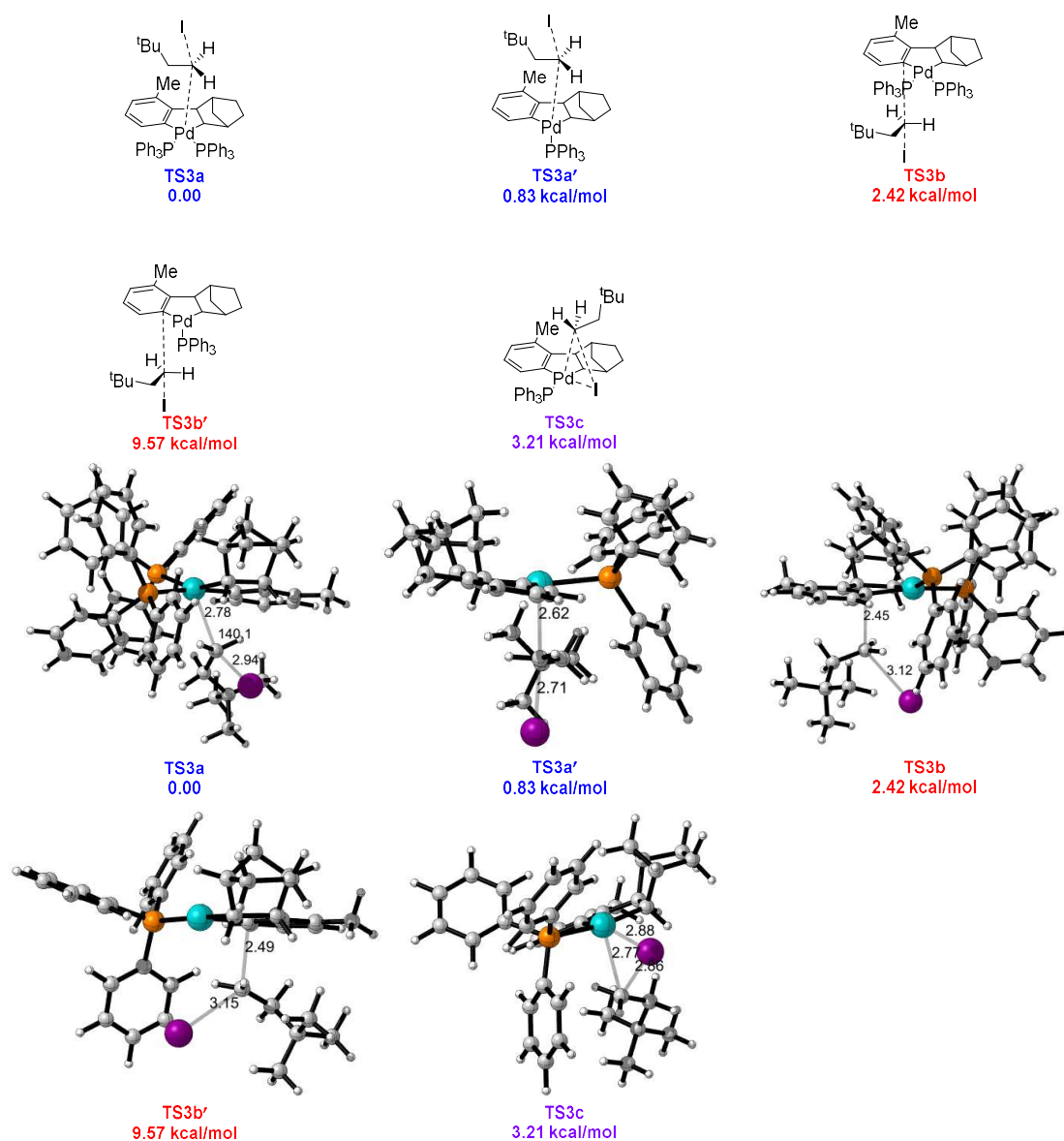


Figure S17. Alkylation transition states of the reaction between *t*-Bu substituted stereochemical probe **1** and palladacycle complex **3** (solvent = MeCN)

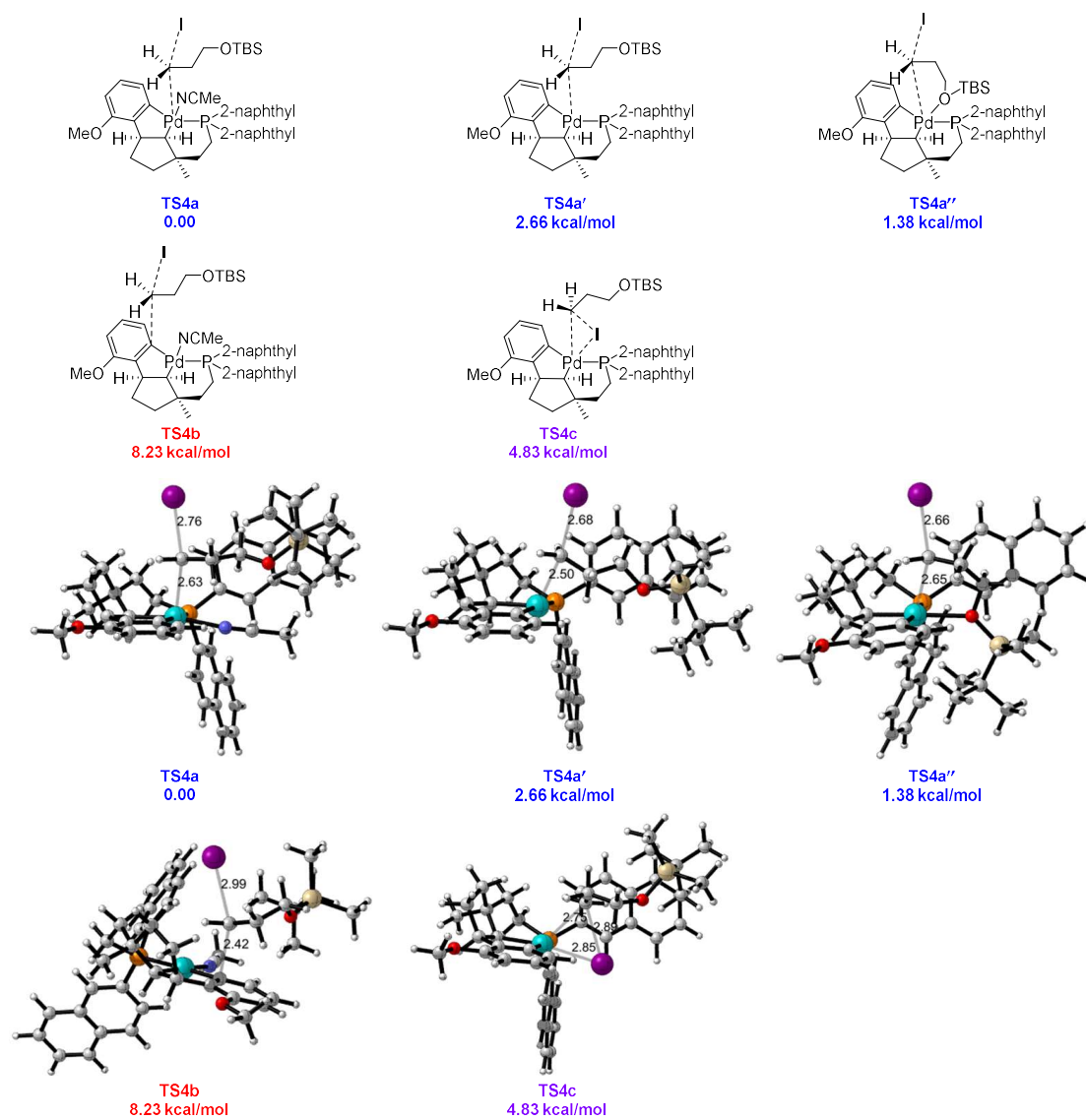


Figure S18. Alkylation transition states of the reaction between TBSO protected stereochemical probe **2** and palladacycle complex **4'** (solvent = MeCN)

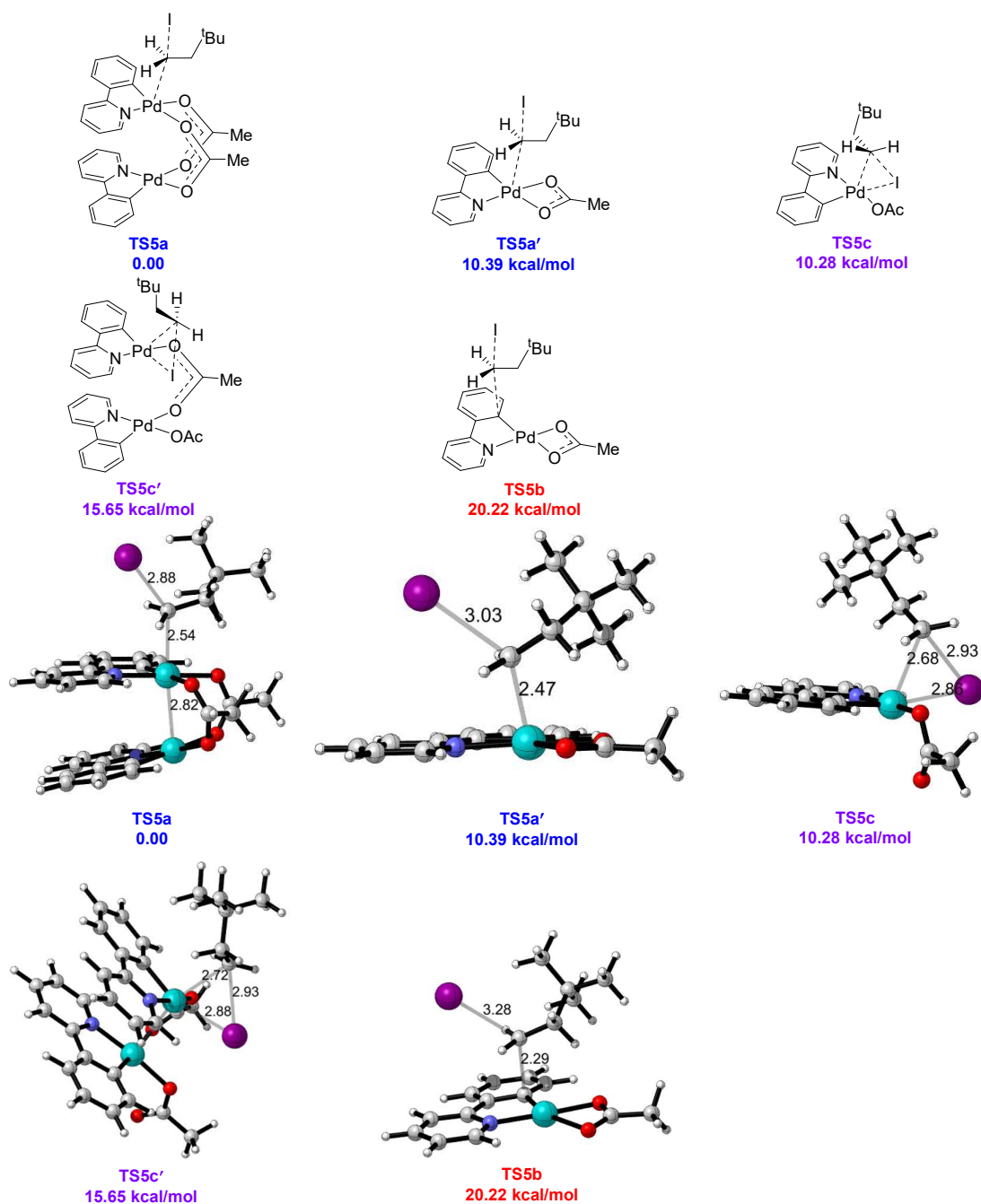


Figure S19. Alkylation transition states of the reaction between *t*-Bu substituted stereochemical probe **1** and palladacycle complex **5** (solvent = *t*-AmylOH/MeCN)

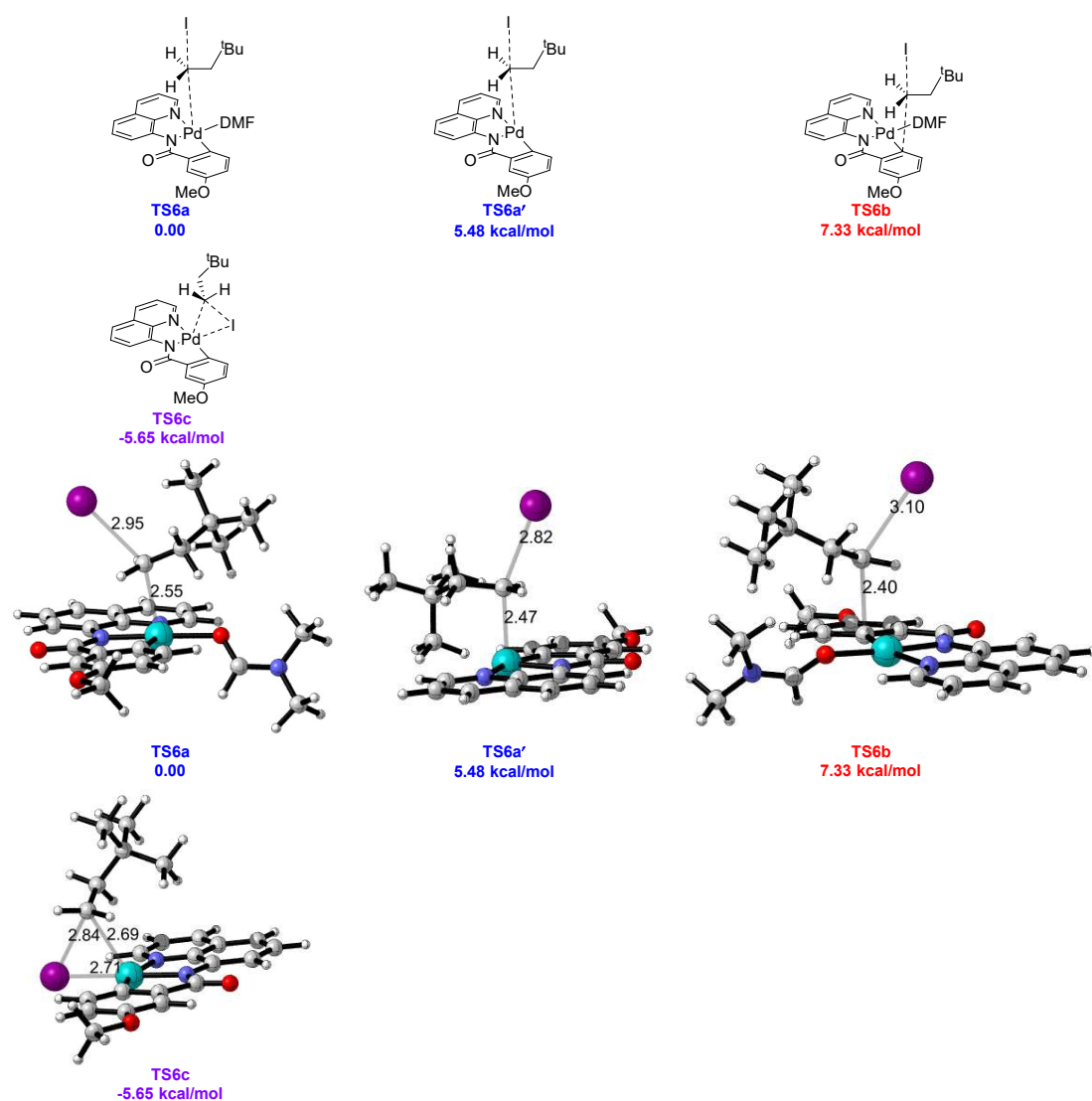


Figure S20. Alkylation transition states of the reaction between *t*-Bu substituted stereochemical probe **1** and palladacycle complex **6'** (solvent = DMF)

5.3 Orbital Energy Level Calculations

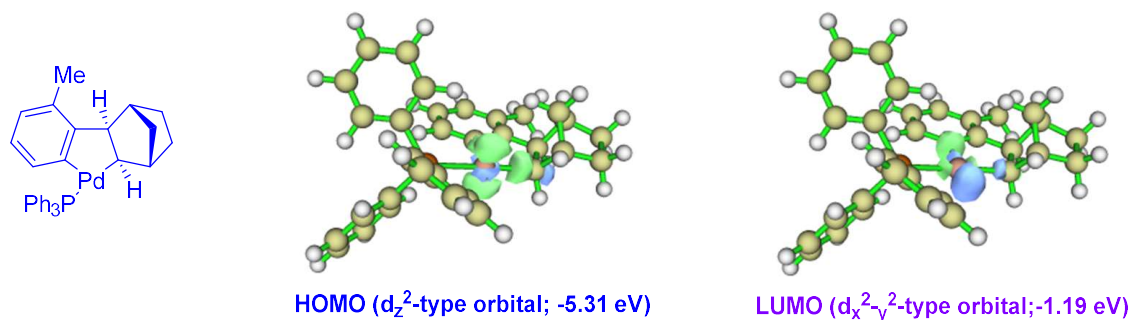


Figure S21. d_z^2 -type and $d_{x^2-y^2}$ -type orbital energy levels of norbornene derived palladacycle complex (isovalue = 0.08)

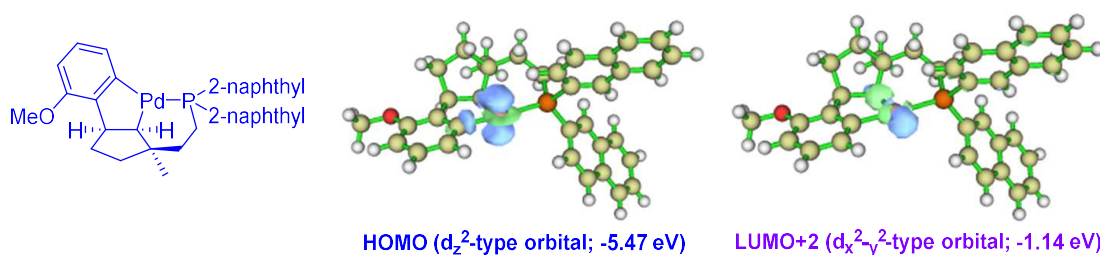


Figure S22. d_z^2 -type and $d_{x^2-y^2}$ -type orbital energy levels of alkene-ligand derived palladacycle complex (isovalue = 0.07)

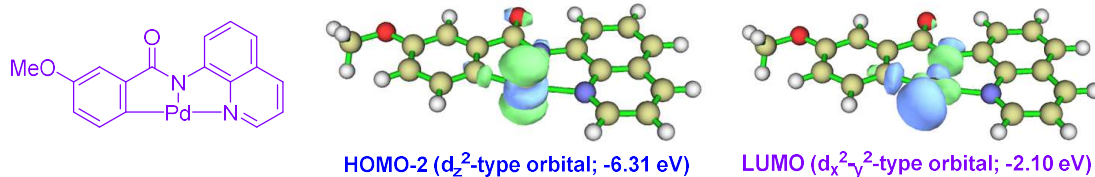


Figure S23. d_z^2 -type and $d_{x^2-y^2}$ -type orbital energy levels of 8-aminoquinoline derived palladacycle complex (isovalue = 0.06)

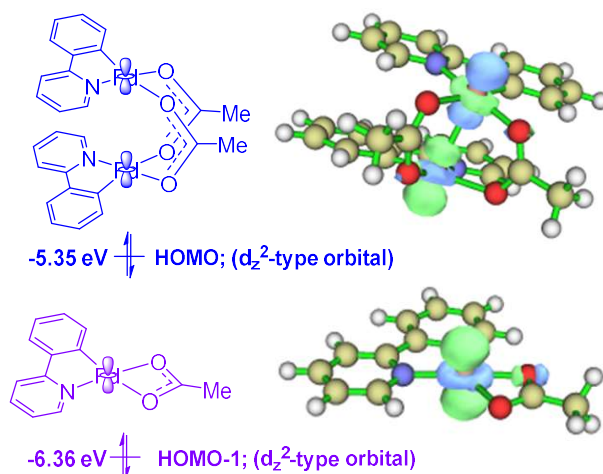


Figure S24. Influence of d^8 - d^8 interaction on the d_z^2 -type orbital energy levels of pyridine coordinated palladacycle complex (isovalue = 0.06)

5.4 Natural Population Analysis and Charge Decomposition Analysis

By selecting the norbornene derived Catellani intermediate **3** and 1-iodo-3,3-dimethyl butane as model compounds, natural population analysis was carried out to study the charge transfer process involved in the alkylation transition state. Compared with reactants, positive charge was deployed on the Pd center while significant negative charge was accumulated on the iodide atom in the S_N2 -type OA transition state (Figure S25a and S25b). This result confirmed the nucleophilicity of the Pd center and the electrophilic nature of alkyl iodide. However, negative charge was accumulated on the Pd center in the stereoretentive OA transition state and the iodide atom was less negative charged (Figure S25c; compared with S_N2 -type OA transition states), indicating the back donation from the iodide atom to the Pd center.

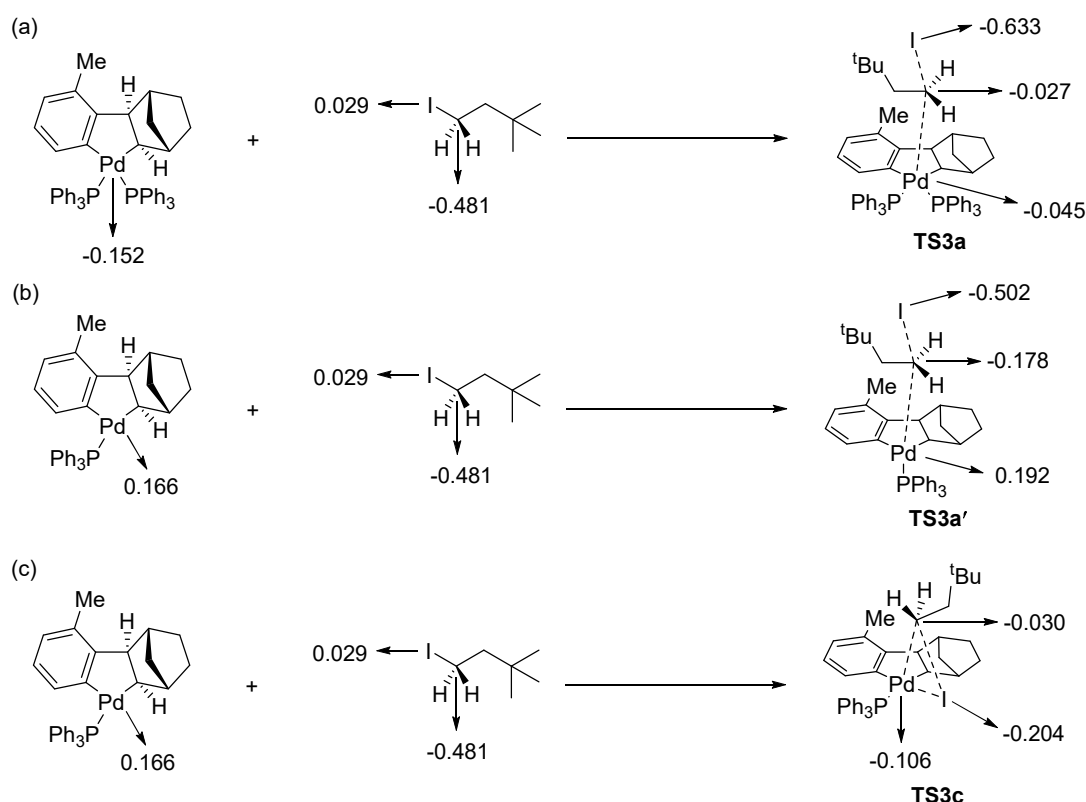
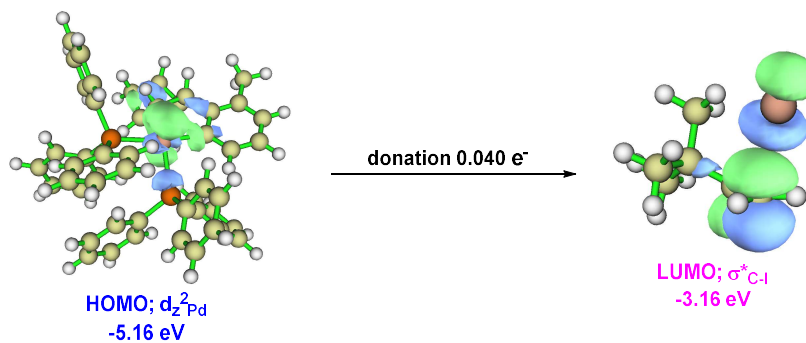


Figure S25. Natural population analysis; atomic charges of Pd, C and I were labeled

To further analysis the donor-acceptor interaction involved in the alkylation transition state, charge decomposition analysis was carried out (Figure S26 – S27):

Important fragment MO pairs involve in the major donor-acceptor interaction of TS3a:



Important fragment MO pairs involve in the major donor-acceptor interaction of TS3a':

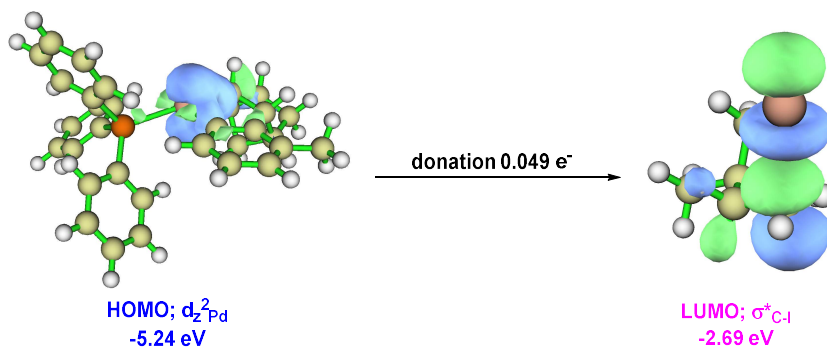


Figure S26. Donor-acceptor interactions involved in TS3a and TS3a' (isovalue = 0.05)

Important fragment MO pairs involve in the major donor-acceptor interaction of TS3c:

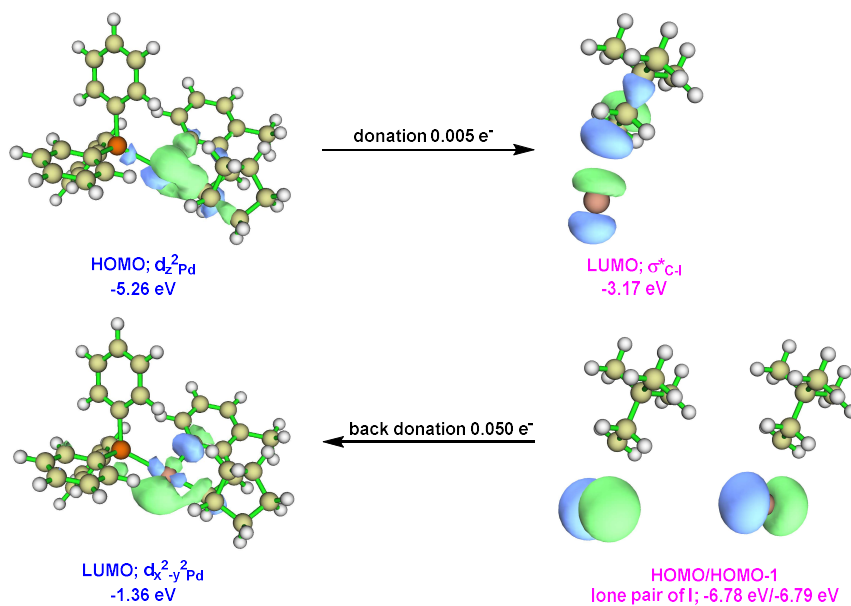


Figure S27. Donor-acceptor interactions involved in TS3c (isovalue = 0.05)

In addition to the results depicted in Figure S26, the back-donation from $\sigma(C-I)$ -type orbital to the empty palladium $d_{x^2-y^2}$ -type orbital was also shown to be significant in TS6c (Figure S28), which we attribute to the lower $d_{x^2-y^2}$ -type orbital energy level of complex 7.

Important fragment MO pairs involve in the major donor-acceptor interaction of TS6c:

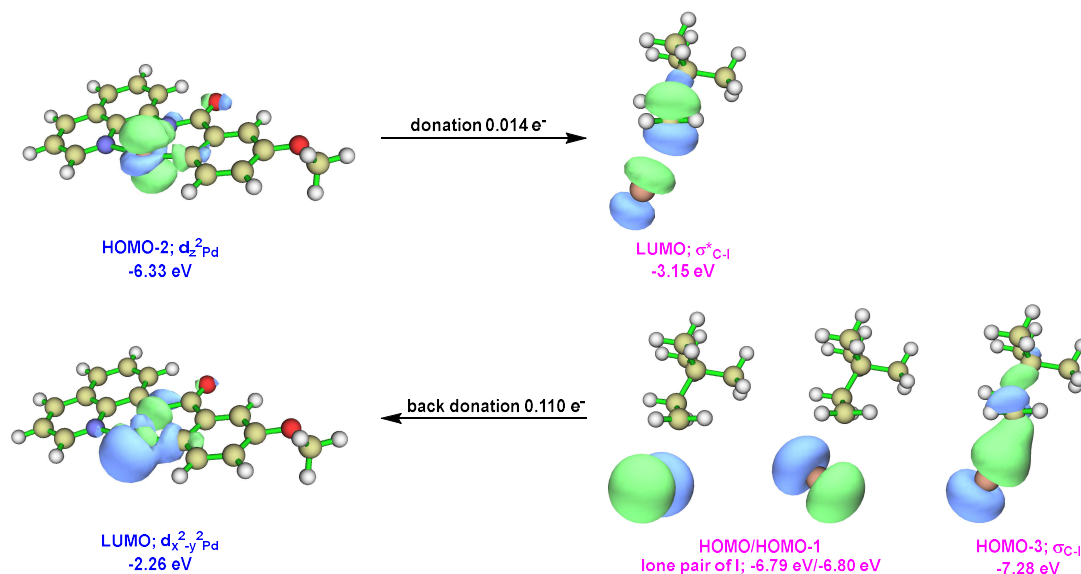


Figure S28. Donor-acceptor interactions involved in TS6c (isovalue = 0.05)

5.5 Ligand Substitution Equilibrium of Complex 5

The ligand substitution equilibrium of complex **5** was calculated and summarized in Figure S29. Our calculation results clearly indicated that substituting one of the acetate ligands in complex **5** by alkyl iodide electrophile is highly unfavored.

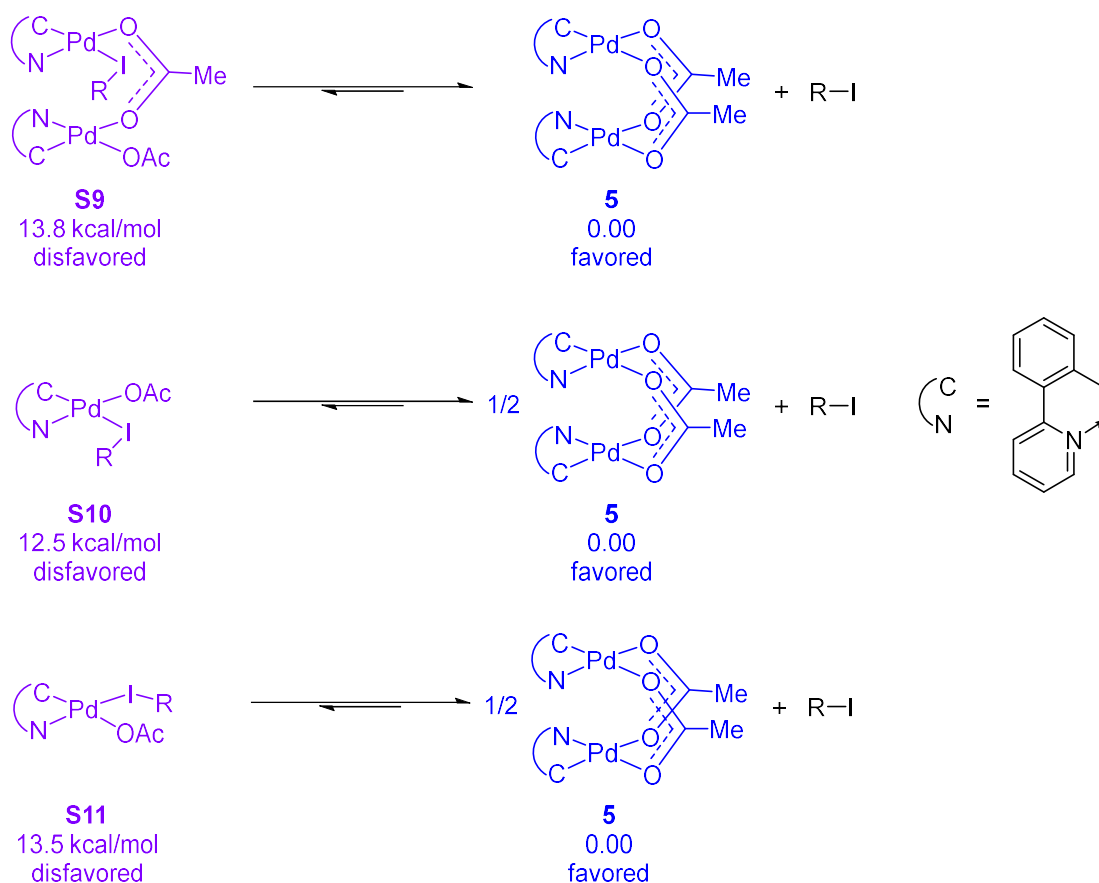


Figure S29. Ligand substitution equilibrium of complex **6** ($R = t\text{-BuCH}_2\text{CH}_2$)

Further analysis on the influence of ligand substitution equilibrium on alkylation mechanism was depicted in Figure S30. Indeed, if we only compared the activation energy barrier of **S11** \rightarrow **TS5a** (21.8 kcal/mol) and **5** + R-I \rightarrow **TS5c** (25.0 kcal/mol), the OA mechanism was favored than the S_N2-type OA on Pd mechanism. However, when ligand substitution equilibrium was added into consideration, the S_N2-type OA on Pd mechanism was favored. Thus, the alkylation product **5a** was formed through stereoinvertive pathway when complex **5** reacted with stereochemical probe.

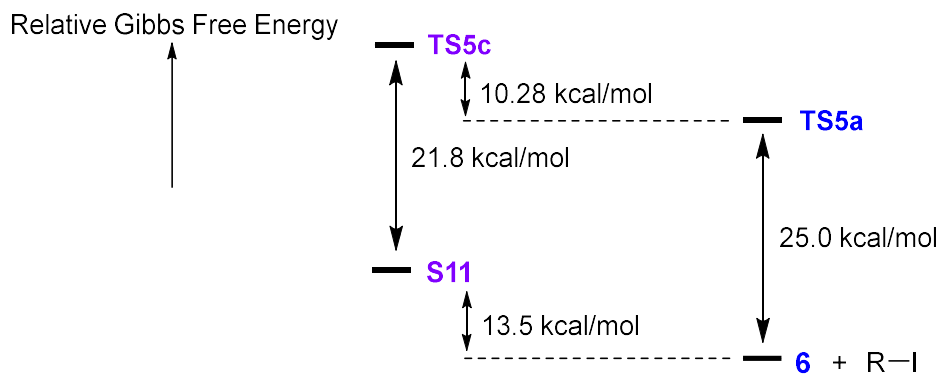


Figure S30. Analysis on the influence of ligand substitution equilibrium on alkylation mechanism (R = *t*-BuCH₂CH₂)

6. NMR Spectra

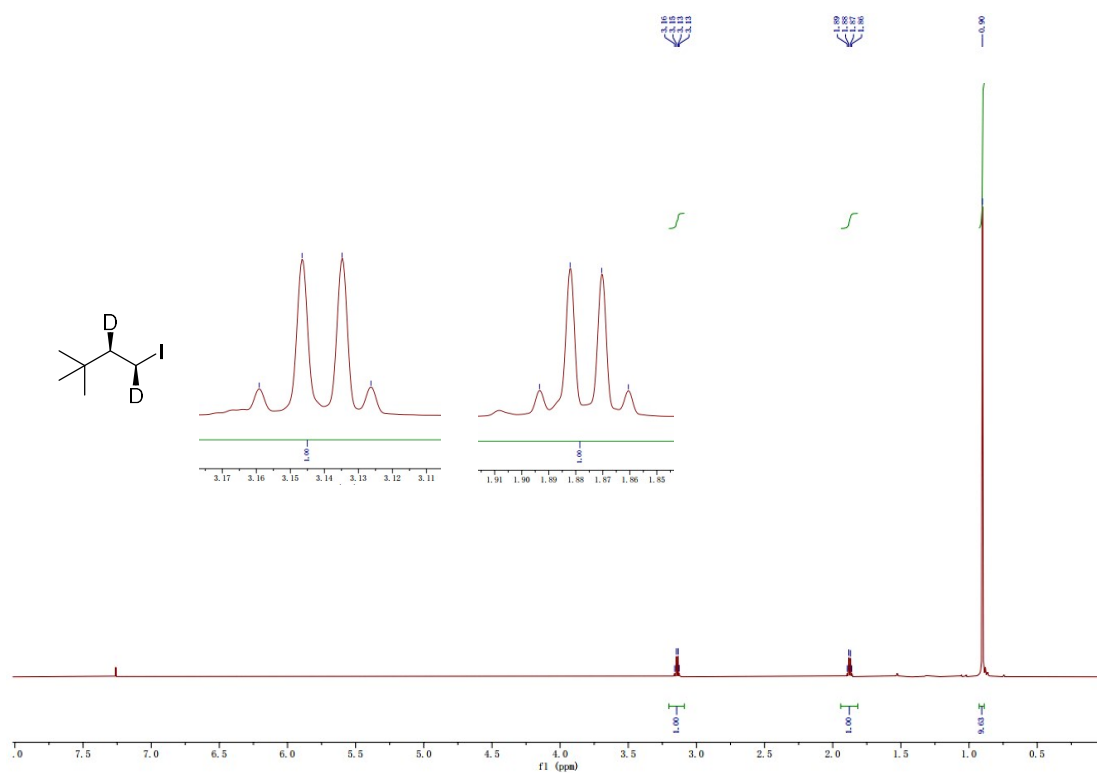


Figure S31. $^1\text{H}\{^2\text{H}\}$ NMR (CDCl₃, 400 MHz) of **1**

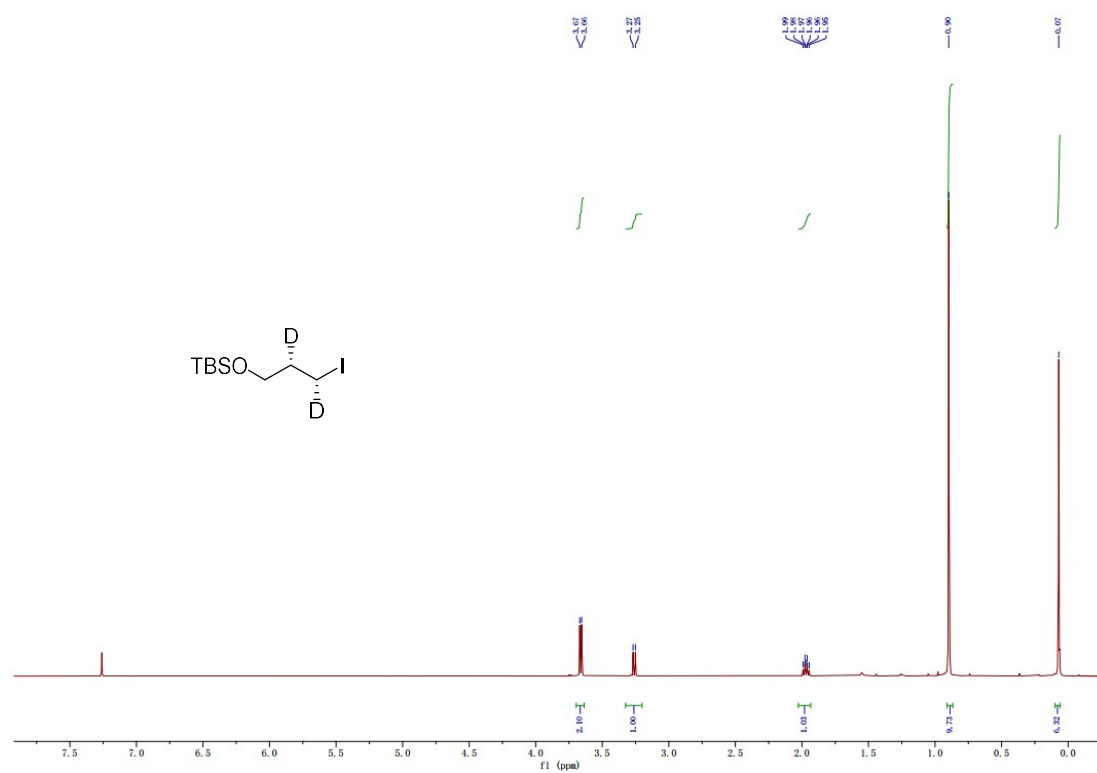


Figure S32. $^1\text{H}\{^2\text{H}\}$ NMR (CDCl₃, 400 MHz) of **2** (*threo*-)

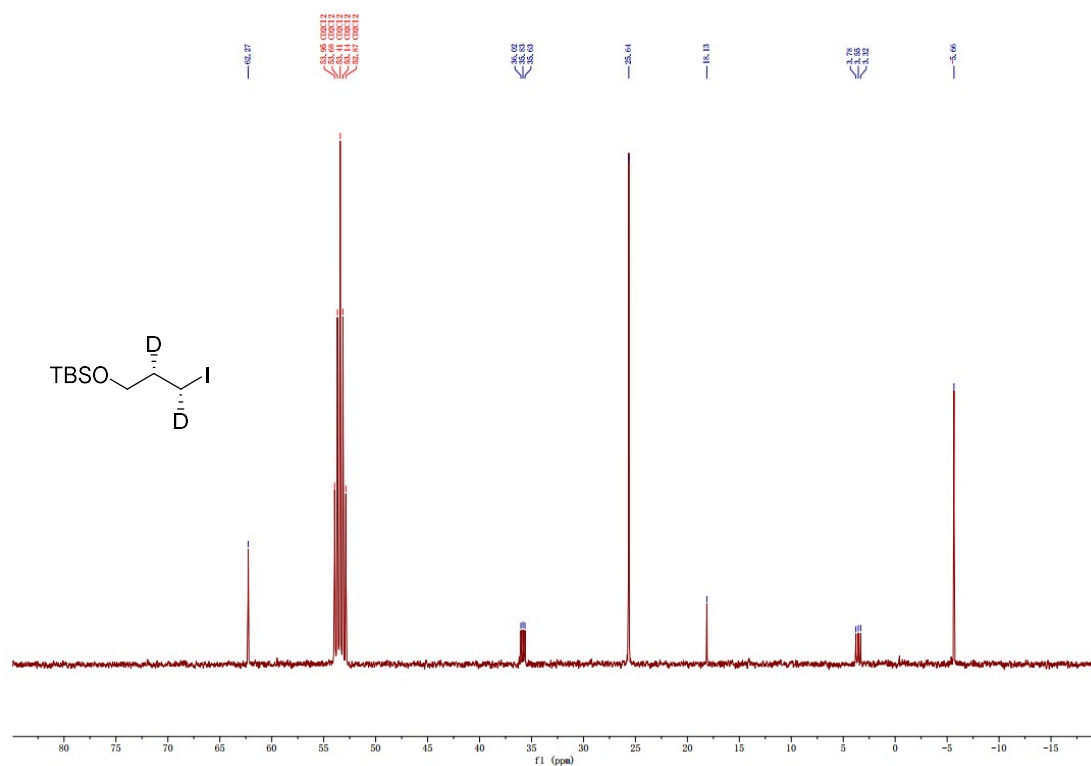


Figure S33. $^{13}\text{C}\{^1\text{H}\}$ NMR (CD₂Cl₂, 101 MHz) of **2** (*threo*-)

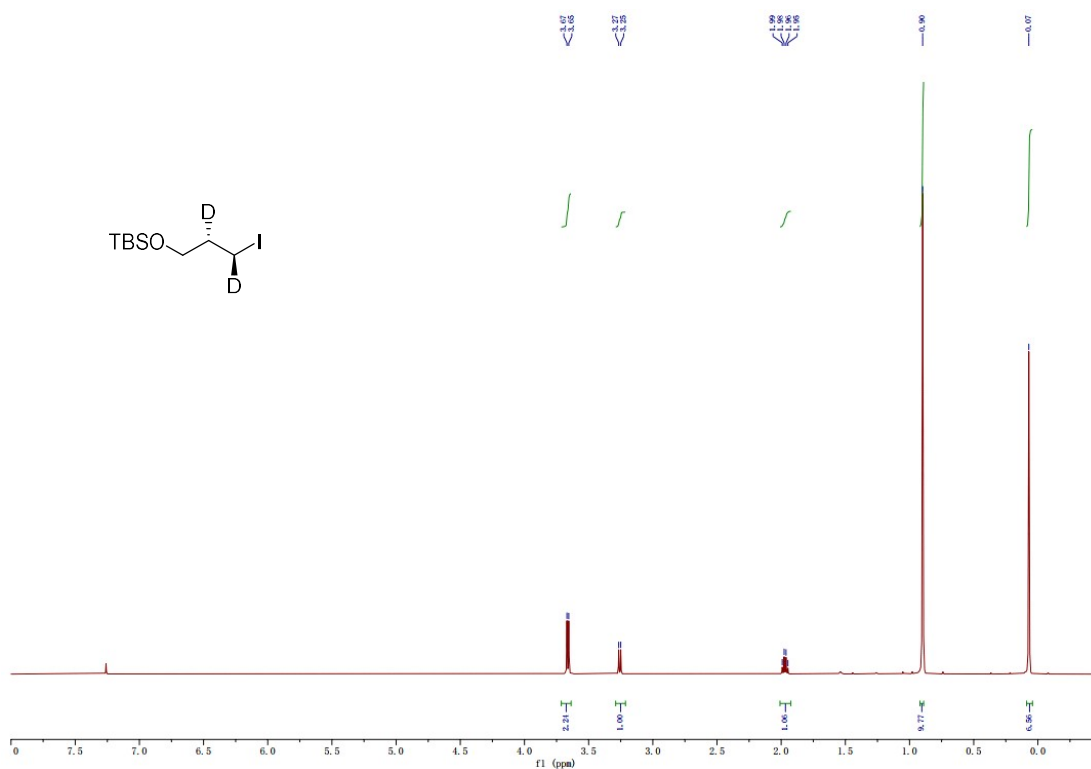


Figure S34. $^1\text{H}\{^2\text{H}\}$ NMR (CDCl₃, 400 MHz) of **2** (*erythro*-)

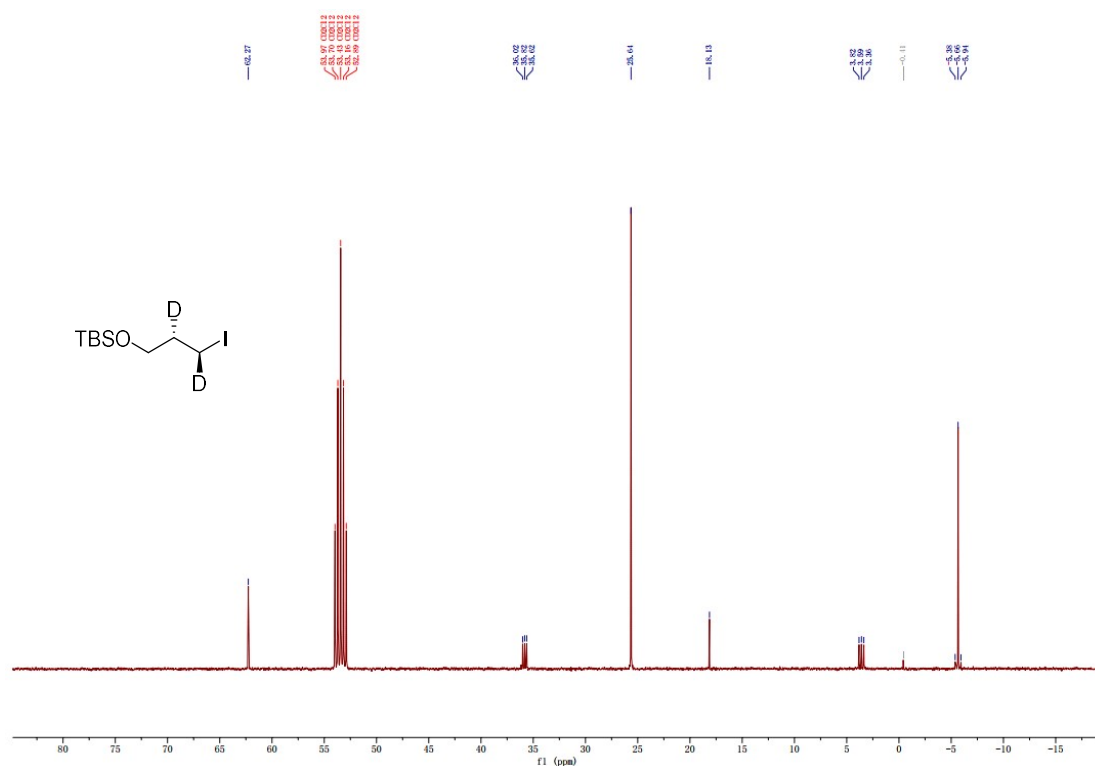


Figure S35. $^{13}\text{C}\{^1\text{H}\}$ NMR (CD_2Cl_2 , 101 MHz) of **2** (*erythro*-)

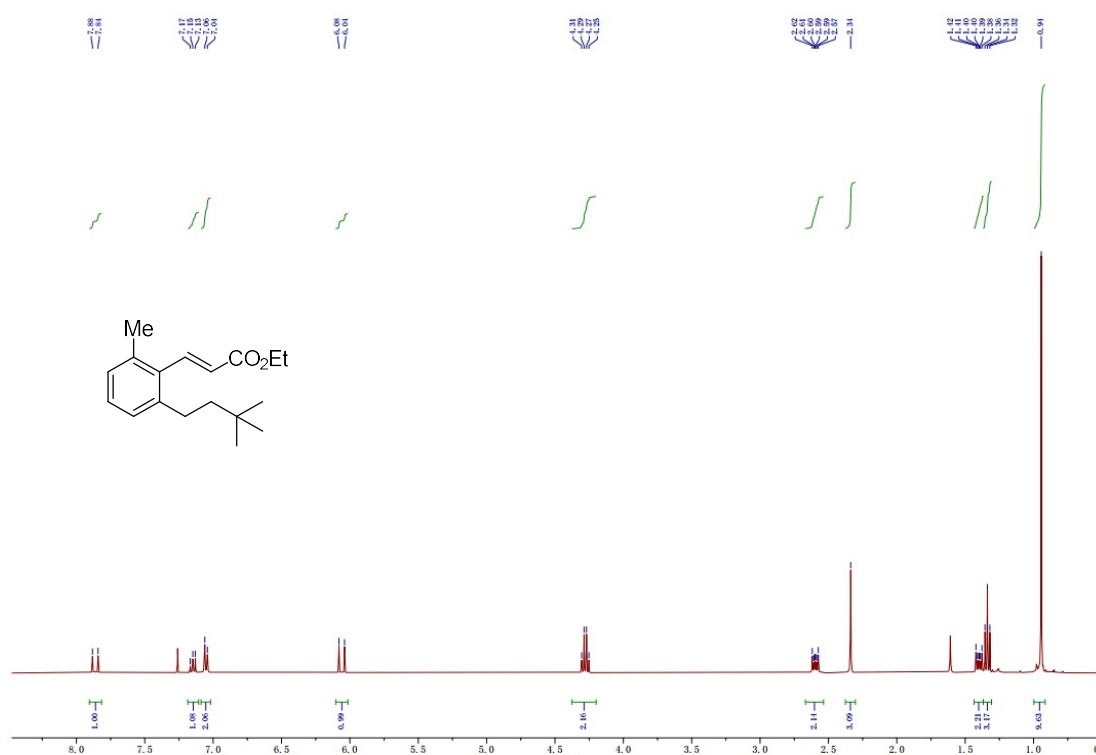


Figure S36. ^1H NMR (CDCl_3 , 400 MHz) of **S3**

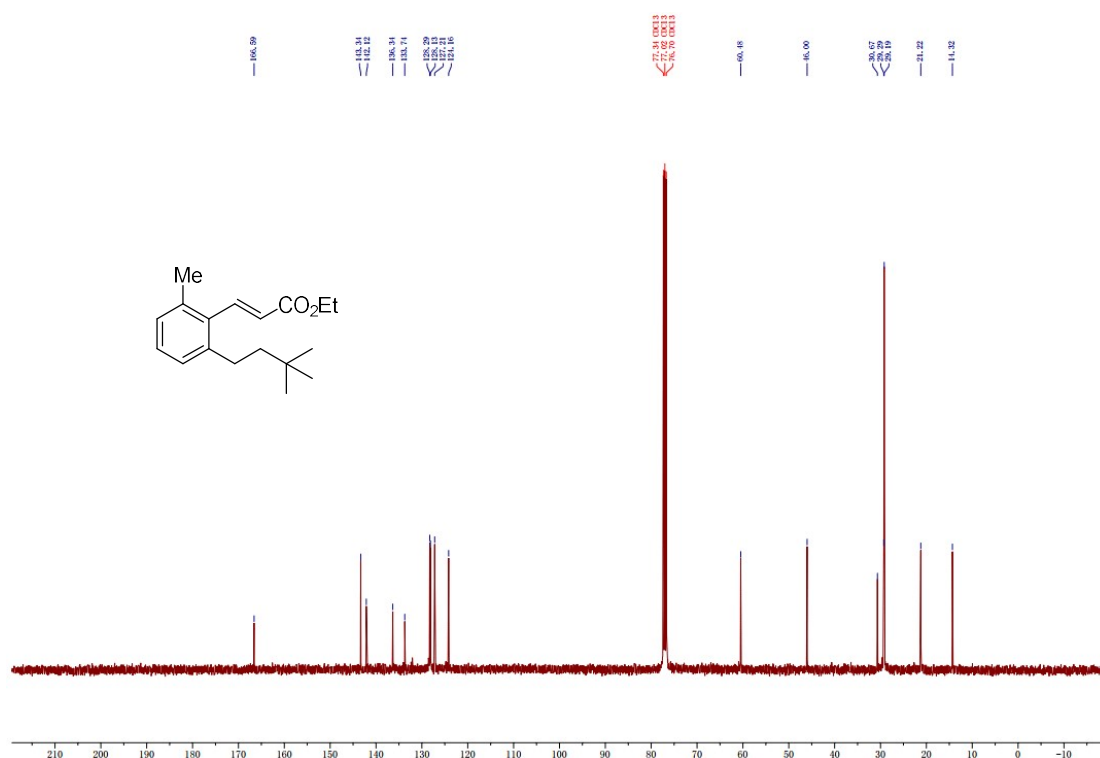


Figure S37. $^{13}\text{C}\{^1\text{H}\}$ NMR (CDCl₃, 101 MHz) of S3

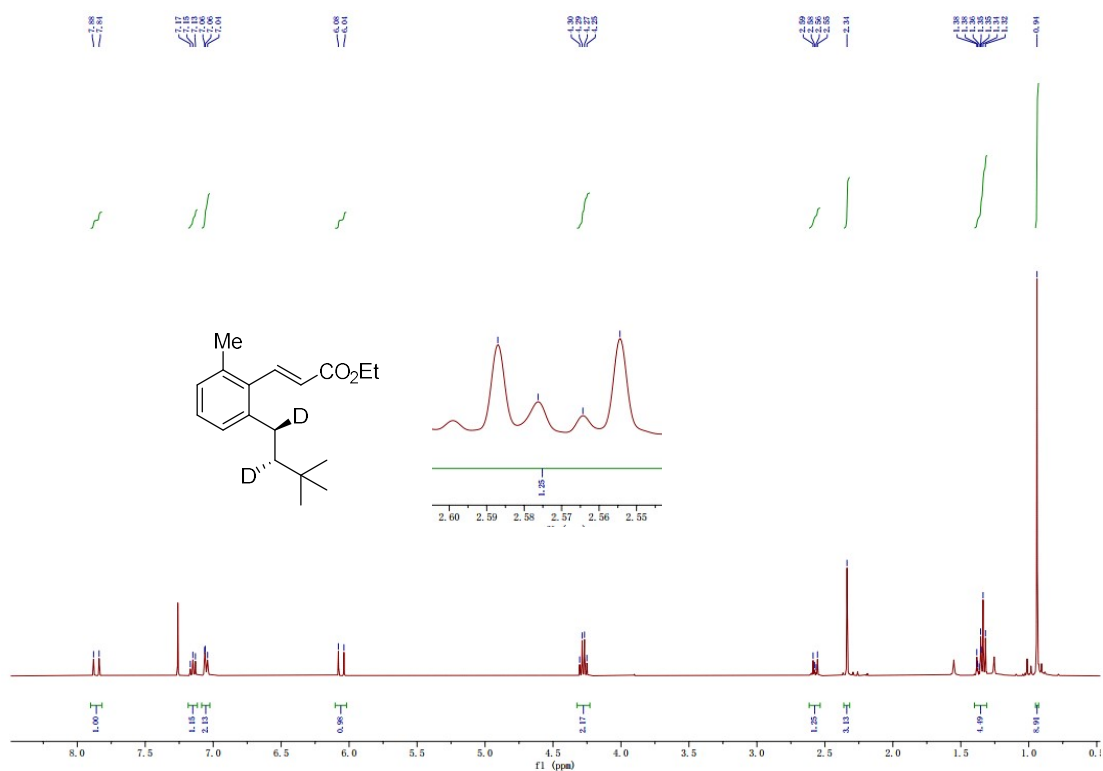


Figure S38. $^1\text{H}\{^2\text{H}\}$ NMR (CDCl₃, 400 MHz) of 3a

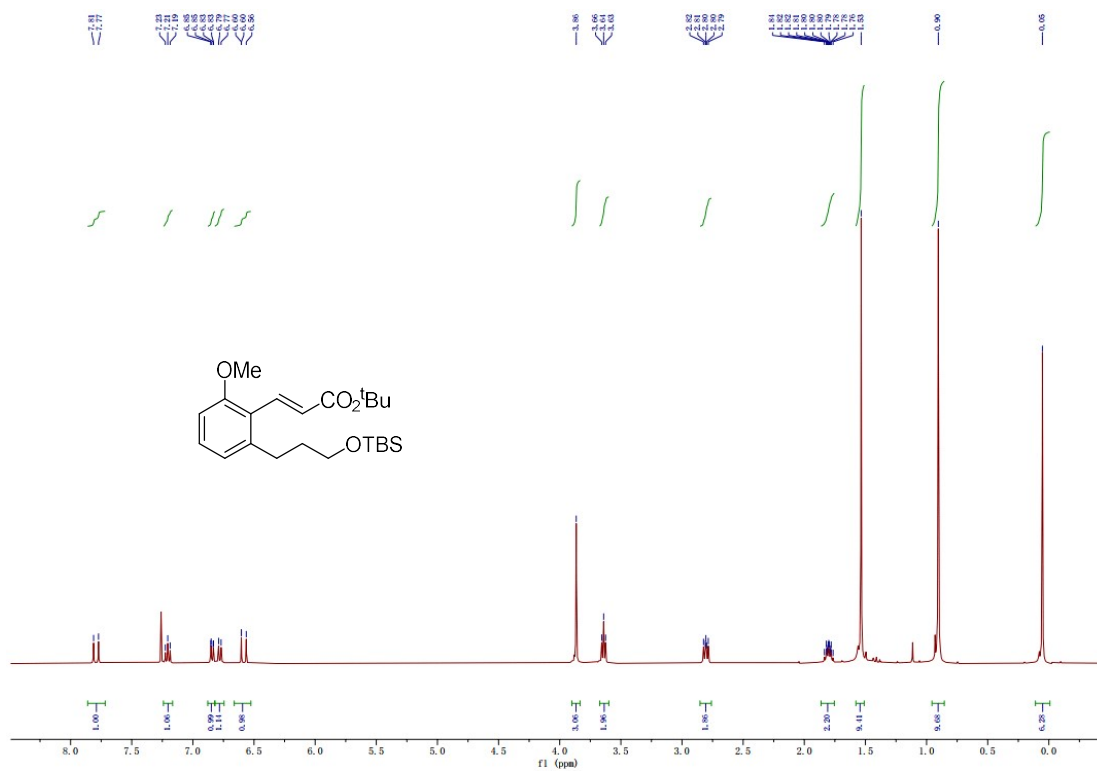


Figure S39. ¹H NMR (CDCl₃, 400 MHz) of S4

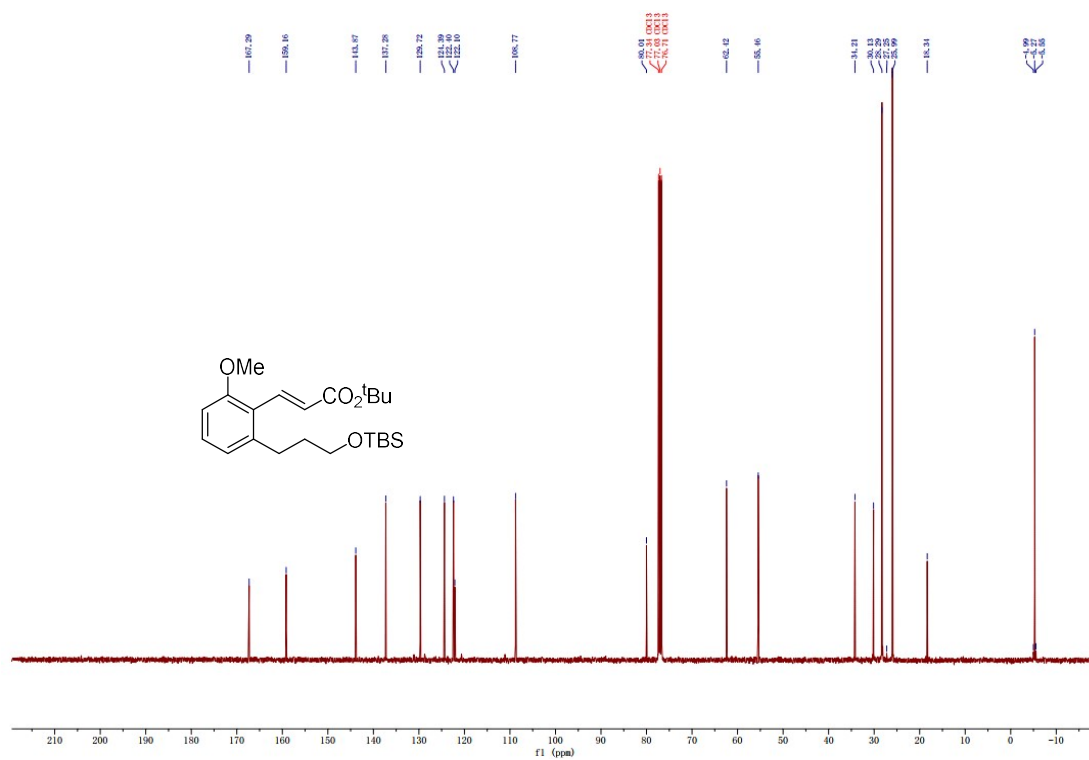


Figure S40. ¹³C{¹H} NMR (CDCl₃, 101 MHz) of S4

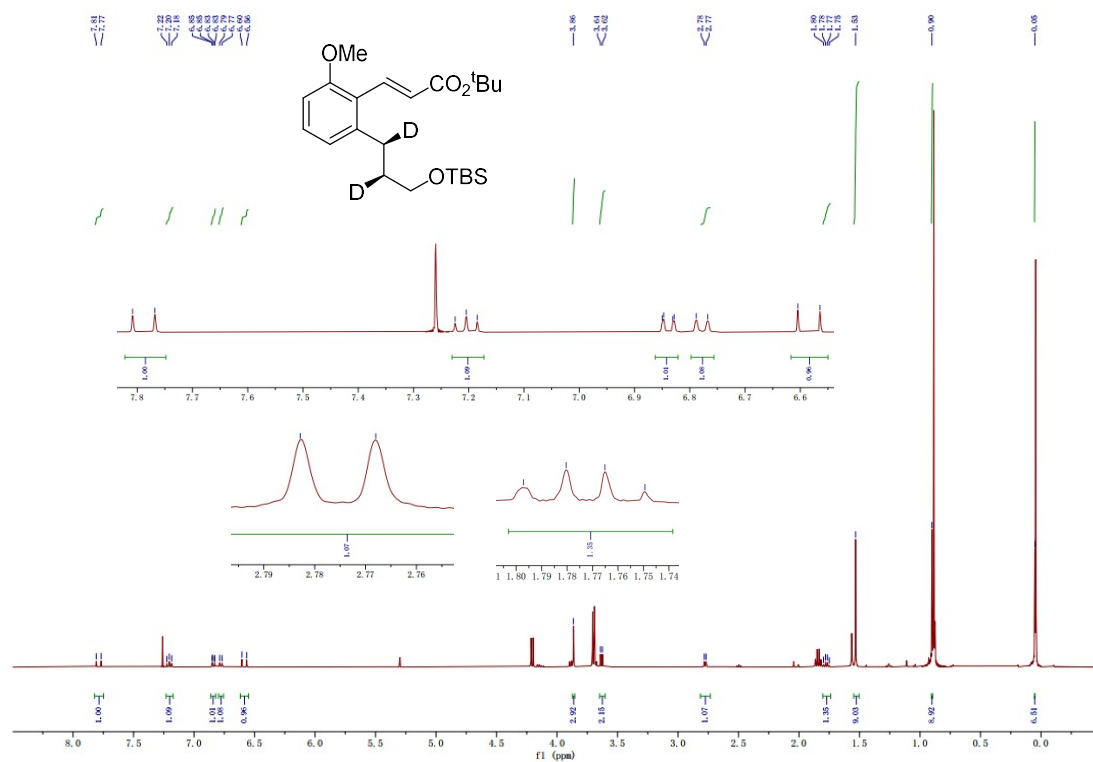


Figure S41. $^1\text{H}\{^2\text{H}\}$ NMR (CDCl₃, 400 MHz) of **4a** (*threo*-)

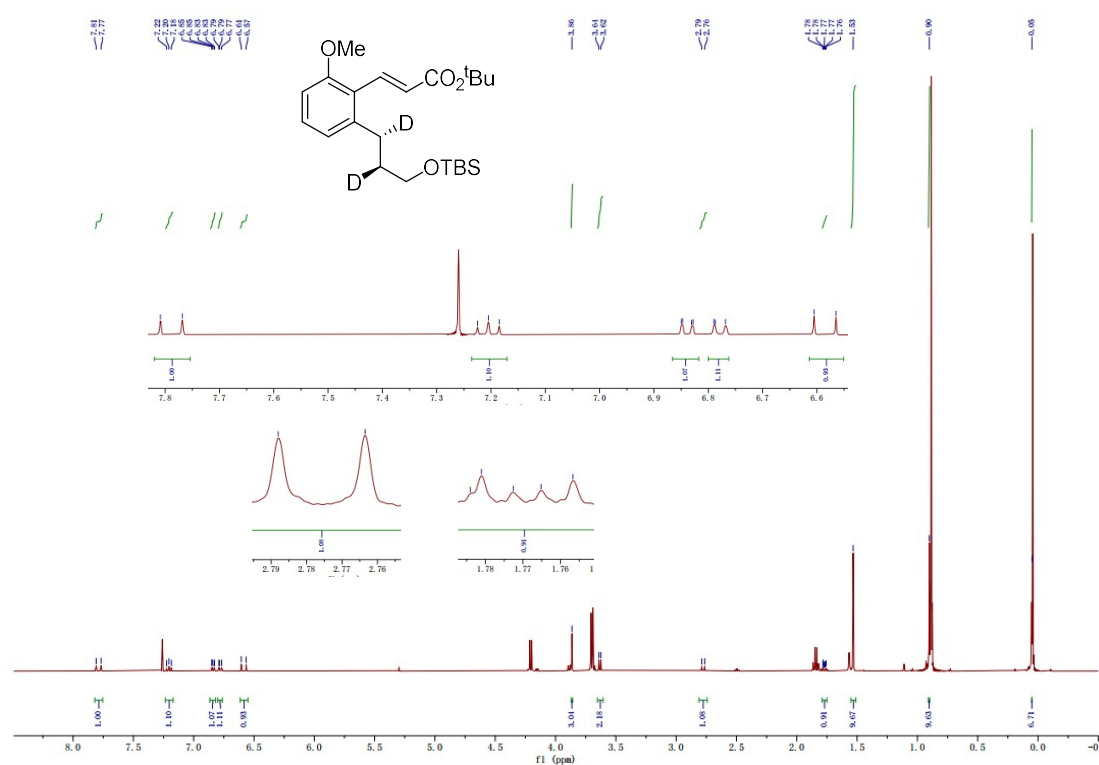


Figure S42. $^1\text{H}\{^2\text{H}\}$ NMR (CDCl₃, 400 MHz) of **4a** (*erythro*-)

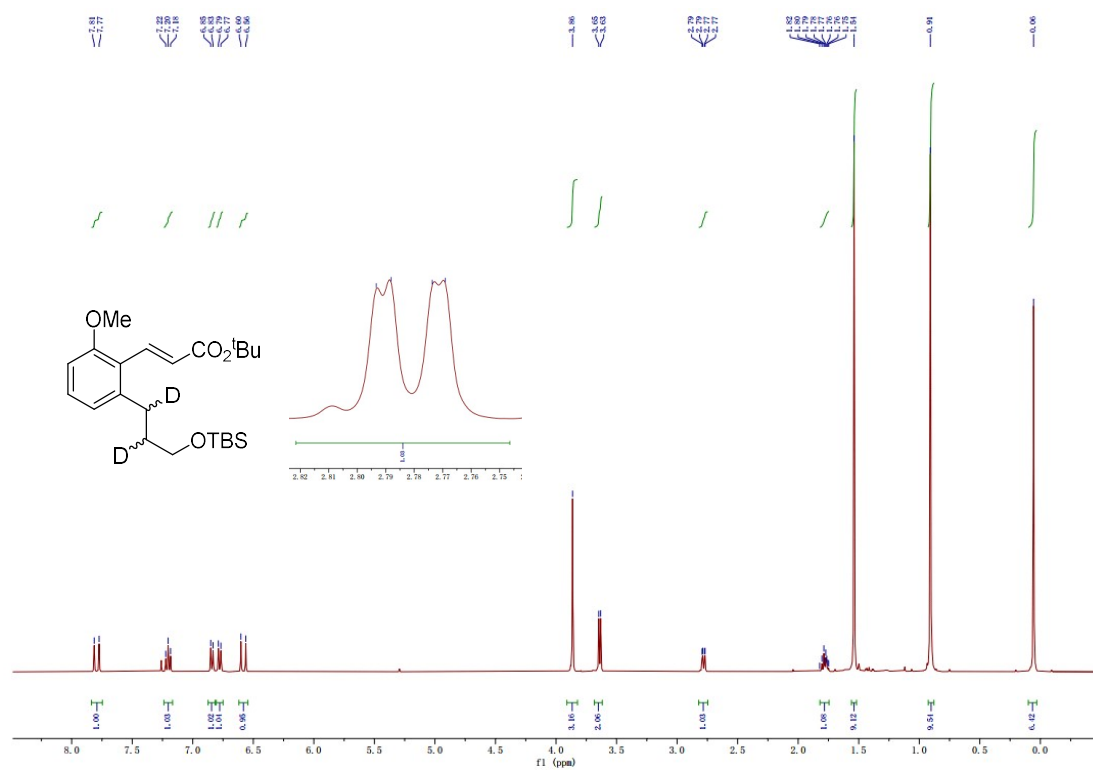


Figure S43. ¹H{²H} NMR (CDCl₃, 400 MHz) of **4a** (threo- and erythro-)

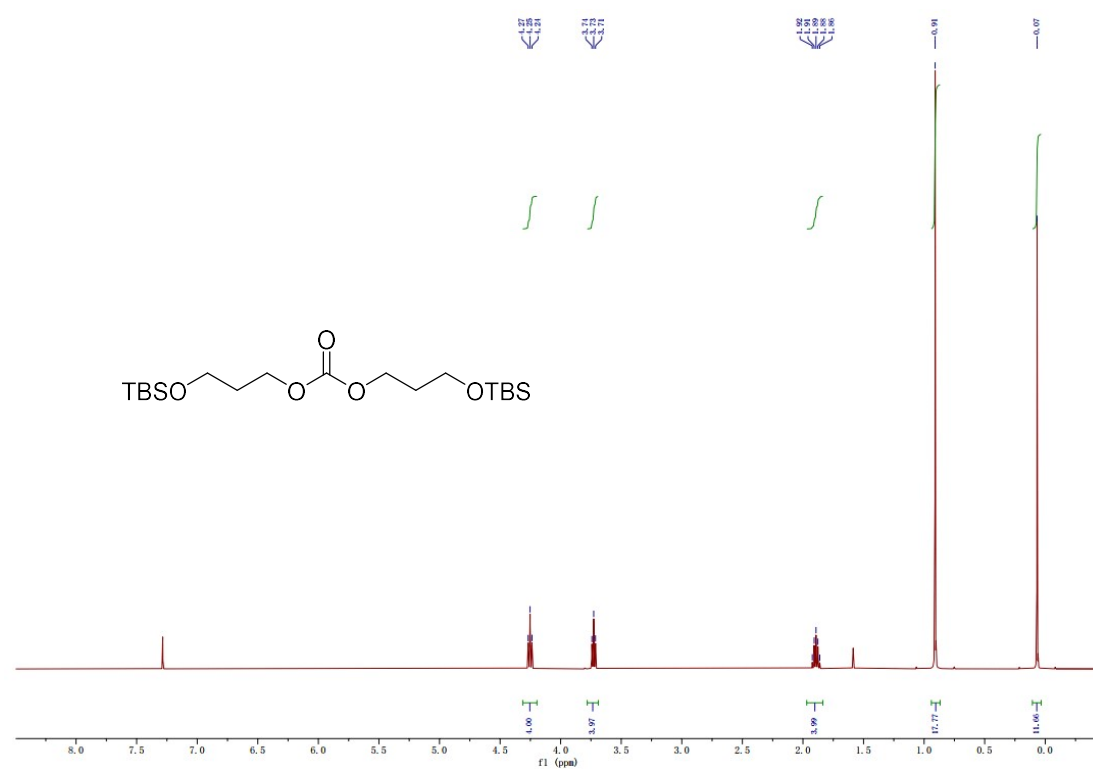


Figure S44. ¹H NMR (CDCl₃, 400 MHz) of **S7**

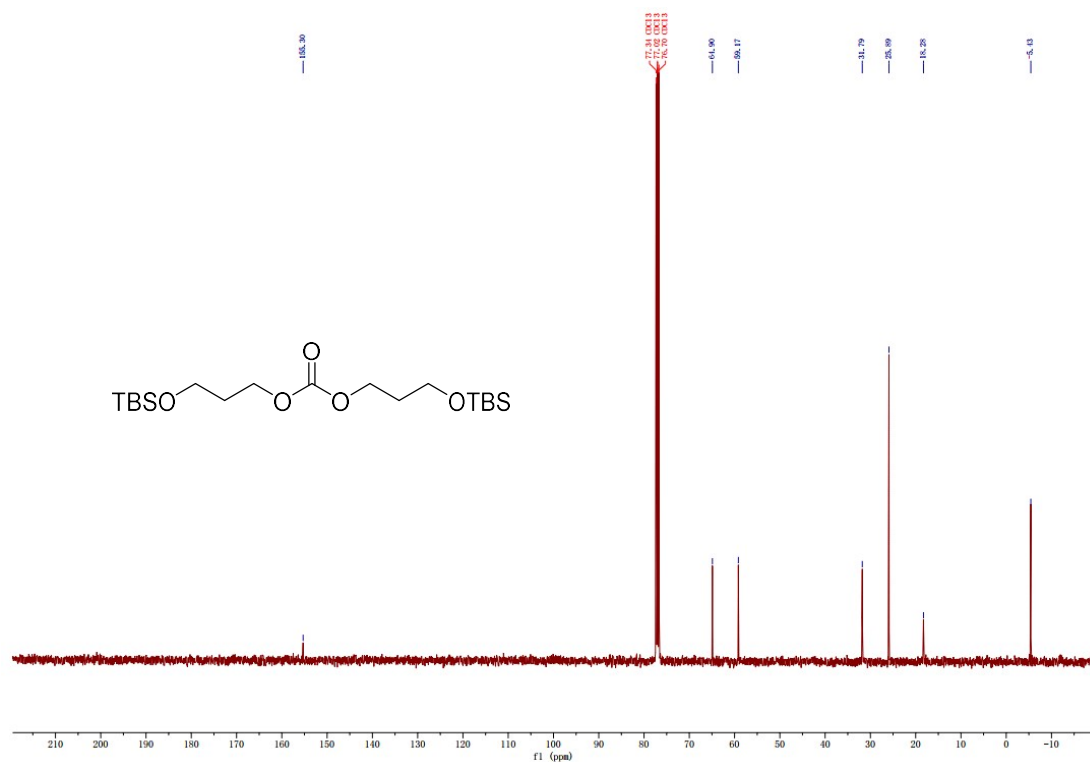


Figure S45. $^{13}\text{C}\{^1\text{H}\}$ NMR (CDCl₃, 101 MHz) of S7

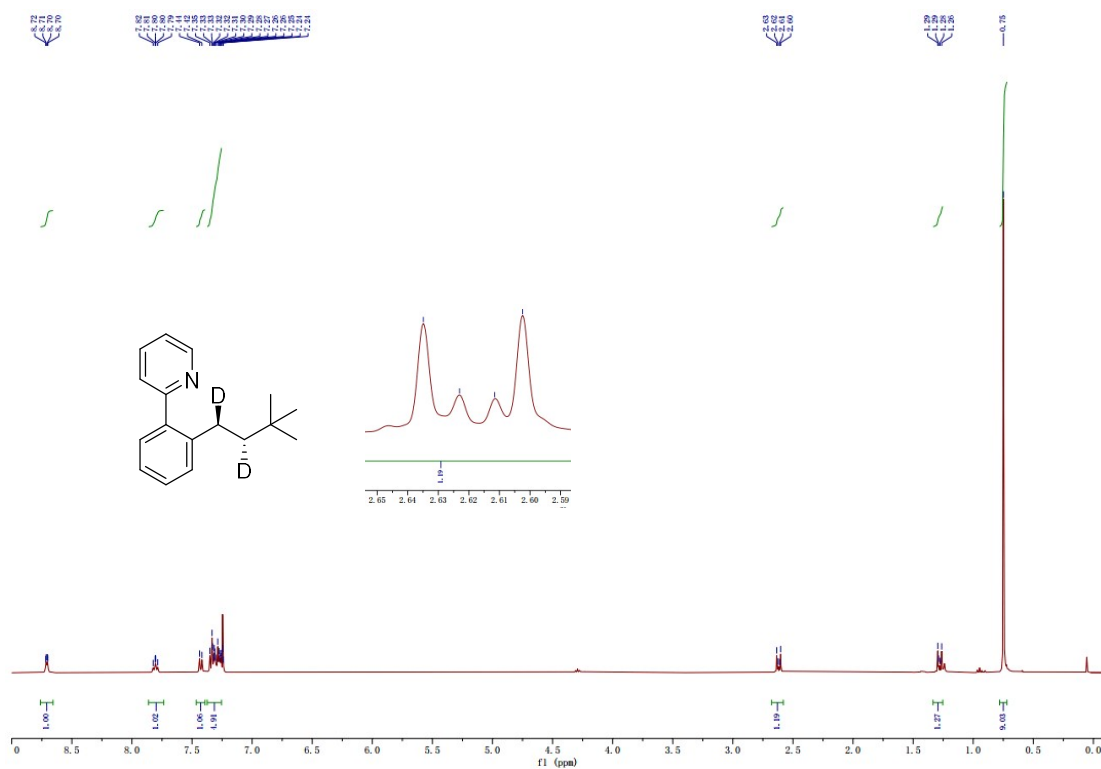


Figure S46. $^1\text{H}\{^2\text{H}\}$ NMR (CDCl₃, 400 MHz) of 5a

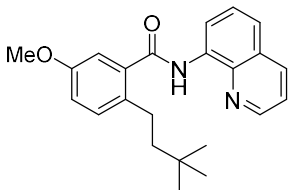


Figure S47. ^1H NMR (CDCl_3 , 400 MHz) of **S5**

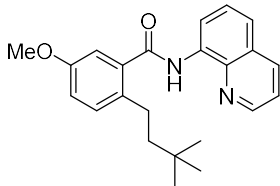


Figure S48. $^{13}\text{C}\{^1\text{H}\}$ NMR (CDCl_3 , 101 MHz) of **S5**

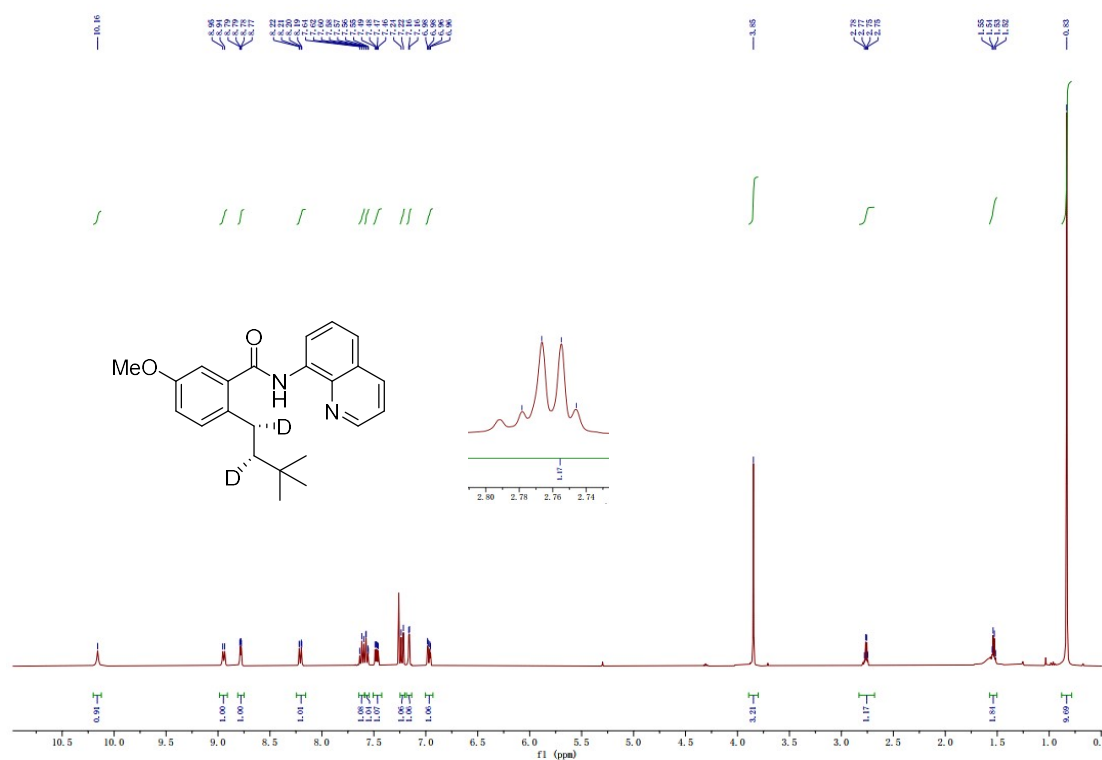


Figure S49. $^1\text{H}\{^2\text{H}\}$ NMR (CDCl_3 , 400 MHz) of **6a**

References

1. Igau, A.; Gladysz, J. A. Reactions of the neohexyl iodide complex $[(\eta^5\text{-C}_5\text{H}_5)\text{Re}(\text{NO})(\text{PPh}_3)(\text{ICH}_2\text{CH}_2\text{C}(\text{CH}_3)_3)]^+\text{BF}_4^-$ and nucleophiles: stereochemistry of carbon-iodine bond cleavage in highly accelerated $\text{S}_{\text{N}}2$ reactions. *Organometallics* **1991**, *10*, 2327–2334.
2. Lei, C.; Jin, X.; Zhou, J. S. Palladium-Catalyzed Heteroarylation and Concomitant ortho-Alkylation of Aryl Iodides. *Angew. Chem. Int. Ed.* **2015**, *54*, 13397–13400.
3. Zhang, S. Y.; Li, Q.; He, G.; Nack, W. A.; Chen, G. Pd-Catalyzed Monoselective ortho-C–H Alkylation of N-Quinolyl Benzamides: Evidence for Stereoretentive Coupling of Secondary Alkyl Iodides. *J. Am. Chem. Soc.* **2015**, *137*, 531–539.
4. Wang, X.; Ji, X.; Shao, C.; Zhang, Y.; Zhang, Y. Palladium-Catalyzed C–H Alkylation of 2-phenylpyridines with Alkyl Iodides. *Org. Biomol. Chem.* **2017**, *15*, 5616–5624.
5. Zheng, Y.-X.; Jiao, L. Hybrid cycloolefin ligands for palladium–olefin cooperative catalysis. *Nat. Synth.* **2022**, *1*, 180–187.
6. (a) Ridgway, B. H.; Woerpel, K. A. Transmetalation of Alkylboranes to Palladium in the Suzuki Coupling Reaction Proceeds with Retention of Stereochemistry. *J. Org. Chem.* **1998**, *63*, 458–460. (b) Orain, D.; Guillemin, J.-C. Synthesis of Functionalized Deuterioallylic Compounds. *J. Org. Chem.* **1999**, *64*, 3563–3566.
7. Han, J.-C.; Liu, L.-Z.; Chang, Y.-Y.; Yue, G.-Z.; Guo, J.; Zhou, L.-Y.; Li, C.-C.; Yang, Z. Asymmetric Total Synthesis of Caribenol A via an Intramolecular Diels–Alder Reaction. *J. Org. Chem.* **2013**, *78*, 5492–5504.
8. (a) Buchwald, S. L.; LaMaire, S. J.; Nielsen, R. B.; Watson, B. T.; King, S. M., A Modified Procedure for the Preparation of $\text{Cp}_2\text{Zr}(\text{H})\text{Cl}$ (Schwartz's Reagent). *Tetrahedron Lett.* **1987**, *28*, 3895–3898. (b) Buchwald, S. L.; LaMaire, S. J.; Nielsen, R. B.; Watson, B. T.; King, S. M., SCHWARTZ'S REAGENT. *Org. Synth.* **1993**, *71*, 77.
9. Begum, S. A.; Terao, J.; Kambe, N. Conversion of $(\text{sp}^3)\text{C}-\text{F}$ Bonds of Alkyl Fluorides to $(\text{sp}^3)\text{C}-\text{Heteroatom}$ (Heteroatom = I, SR, SeR, TeR) Bonds by the Use of Magnesium Reagents Having Heteroatom Substituents. *Chem. Lett.* **2007**, *36*, 196–197.
10. Collman, J. P.; Brauman, J. I.; Madonik, A. M. Oxidative Addition Mechanisms of a Four-Coordinate Rhodium (I) Macrocyclic. *Organometallics* **1986**, *5*, 310–322.
11. (a) Yang, G. K.; Bergman, R. G. Stereochemistry of metallacycle formation in the double alkylation of bis(triphenylphosphine)nitrogen(1+) bis(η^5 -cyclopentadienyl)-di- μ -carbonyldicobaltate with α,γ -diiodoalkanes. *J. Am. Chem. Soc.* **1983**, *105*, 6045–6052. (b) Luo, Y.-C.; Yang, C.; Qiu, S.-Q.; Liang, Q.-J.; Xu, Y.-H.; Loh, T.-P. Palladium(II)-Catalyzed Stereospecific Alkenyl C–H Bond Alkylation of Allylamines with Alkyl Iodides. *ACS Catal.* **2019**, *9*, 4271–4276.
12. Carcache, D. A.; Cho, Y. S.; Hua, Z.; Tian, Y.; Li, Y.-M.; Danishefsky, S. J. Total Synthesis of (\pm)-Jiadifenin and Studies Directed to Understanding Its SAR: Probing Mechanistic and Stereochemical Issues in Palladium-Mediated Allylation of Enolate-Like Structures. *J. Am. Chem. Soc.* **2006**, *128*, 1016–1022.
13. Murray, B.; Zhao, S.; Aramini, J. M.; Wang, H.; Biscoe, M. R. The Stereochemical Course of Pd-Catalyzed Suzuki Reactions Using Primary Alkyltrifluoroborate Nucleophiles. *ACS Catal.* **2021**, *11*, 2504–2510.
14. Gaussian 16, Revision A.03, M. J. Frisch, G. W. Trucks, H. B. Schlegel, G. E. Scuseria, M. A. Robb, J. R. Cheeseman, G. Scalmani, V. Barone, G. A. Petersson, H. Nakatsuji, X. Li, M. Caricato,

- A. V. Marenich, J. Bloino, B. G. Janesko, R. Gomperts, B. Mennucci, H. P. Hratchian, J. V. Ortiz, A. F. Izmaylov, J. L. Sonnenberg, D. Williams-Young, F. Ding, F. Lipparini, F. Egidi, J. Goings, B. Peng, A. Petrone, T. Henderson, D. Ranasinghe, V. G. Zakrzewski, J. Gao, N. Rega, G. Zheng, W. Liang, M. Hada, M. Ehara, K. Toyota, R. Fukuda, J. Hasegawa, M. Ishida, T. Nakajima, Y. Honda, O. Kitao, H. Nakai, T. Vreven, K. Throssell, J. A. Montgomery, Jr., J. E. Peralta, F. Ogliaro, M. J. Bearpark, J. J. Heyd, E. N. Brothers, K. N. Kudin, V. N. Staroverov, T. A. Keith, R. Kobayashi, J. Normand, K. Raghavachari, A. P. Rendell, J. C. Burant, S. S. Iyengar, J. Tomasi, M. Cossi, J. M. Millam, M. Klene, C. Adamo, R. Cammi, J. W. Ochterski, R. L. Martin, K. Morokuma, O. Farkas, J. B. Foresman, and D. J. Fox, Gaussian, Inc., Wallingford CT, 2016.
15. Zhao, Y.; Truhlar, D. G. The M06 suite of density functionals for main group thermochemistry, thermochemical kinetics, noncovalent interactions, excited states, and transition elements: two new functionals and systematic testing of four M06-class functionals and 12 other functionals. *Theor. Chem. Acc.* **2008**, *120*, 215–241.
16. Marenich A. V.; Cramer C. J.; Truhlar D. G. Universal solvation model based on solute electron density and on a continuum model of the solvent defined by the bulk dielectric constant and atomic surface tensions. *J. Phys. Chem. B* **2009**, *113*, 6378–6396.
17. (a) Dolg, M.; Wedig, U.; Stoll, H.; Preuss, H. Energy-adjusted ab initio pseudopotentials for the first row transition elements. *J. Chem. Phys.* **1987**, *86*, 866–872. (b) Andrae, D.; Häußermann, U.; Dolg, M.; Stoll, H.; Preuß, H. Energy-adjusted ab initio pseudopotentials for the second and third row transition elements. *Theor. Chem. Acc.* **1990**, *77*, 123–141.
18. Krishnan, R.; Binkley, J. S.; Seeger, R.; Pople, J. A. Self-consistent molecular orbital methods. XX. A basis set for correlated wave functions. *J. Chem. Phys.* **1980**, *72*, 650–654.
19. (a) Becke, A. D. Density-functional thermochemistry. III. The role of exact exchange. *J. Chem. Phys.* **1993**, *98*, 5648–5652. (b) Lee, C.; Yang, W.; Parr, R. G. Development of the Colle-Salvetti correlation-energy formula into a functional of the electron density. *Phys. Rev. B: Condens. Matter Mater. Phys.* **1988**, *37*, 785–789. (c) Stephens, P. J.; Devlin, F. J.; Chabalowski, C. F.; Frisch, M. J. Ab Initio Calculation of Vibrational Absorption and Circular Dichroism Spectra Using Density Functional Force Fields. *J. Phys. Chem.* **1994**, *98*, 11623–11627.
20. (a) Grimme, S.; Antony, J.; Ehrlich, S.; Krieg, H. A consistent and accurate ab initio parametrization of density functional dispersion correction (DFT-D) for the 94 elements H-Pu. *J. Chem. Phys.* **2010**, *132*, 154104–154119. (b) Grimme, S.; Ehrlich, S.; Goerigk, L. Effect of the damping function in dispersion corrected density functional theory. *J. Comput. Chem.* **2011**, *32*, 1456–1465.
21. (a) Hay, P. J.; Wadt, W. R. Ab initio effective core potentials for molecular calculations. Potentials for K to Au including the outermost core orbitals. *J. Chem. Phys.* **1985**, *82*, 299–310. (b) Ehlers, A. W.; Böhm, M.; Dapprich, S.; Gobbi, A.; Höllwarth, A.; Jonas, V.; Köhler, K. F.; Stegmann, R.; Veldkamp, A.; Frenking, G. *Chem. Phys. Lett.* **1993**, *208*, 111–114. (c) Roy, L. E.; Hay, P. J.; Martin, R. L. Revised Basis Sets for the LANL Effective Core Potentials. *J. Chem. Theory Comput.* **2008**, *4*, 1029–1031.
22. (a) Ditchfield, R.; Hehre, W. J.; Pople, J. A. Self-Consistent Molecular-Orbital Methods. IX. An Extended Gaussian-Type Basis for Molecular-Orbital Studies of Organic Molecules. *J. Chem. Phys.* **1971**, *54*, 724–728. (b) Hehre, W. J.; Ditchfield, R.; Pople, J. A. Self-Consistent Molecular Orbital Methods. XII. Further Extensions of Gaussian-Type Basis Sets for Use in Molecular Orbital Studies of Organic Molecules. *J. Chem. Phys.* **1972**, *56*, 2257–2261. (c) Hariharan, P. C.; Pople, J. A. The

- influence of polarization functions on molecular orbital hydrogenation energies. *Theor. Chim. Acta.* **1973**, 28, 213–222.
23. (a) Strotman, N. A.; Ortiz, A.; Savage, S. A.; Wilbert, C. R.; Ayers, S.; Kiao, S. Revisiting a Classic Transformation: A Lossen Rearrangement Initiated by Nitriles and “Pseudo-Catalytic” in Isocyanate. *J. Org. Chem.* **2017**, 82, 4044–4049. (b) Minnesota Solvent Descriptor Database: <https://comp.chem.umn.edu/solvation/mnsddb.pdf>
24. Reed, A. E.; Weinstock, R. B.; Weinhold, F. Natural population analysis. *J. Chem. Phys.* **1985**, 83, 735–746.
25. (a) Dapprich, S.; Frenking, G. Investigation of Donor-Acceptor Interactions: A Charge Decomposition Analysis Using Fragment Molecular Orbitals. *J. Phys. Chem.* **1995**, 99, 9352–9362. (b) Meng Xiao, Tian Lu, Generalized Charge Decomposition Analysis (GCDA) Method, *Journal of Advances in Physical Chemistry*, **2015**, 4, 111–124.
26. Tian Lu, Feiwu Chen, Multiwfn: A Multifunctional Wavefunction Analyzer, *J. Comput. Chem.* **2012**, 33, 580–592.
27. CYLview20; Legault, C. Y., Université de Sherbrooke, 2020 (<http://www.cylview.org>).